AD-A066 839 WEATHER WING (1ST) HICKAM AFB HI F/G 4/2
THE ROLE OF ATMOSPHERIC TIDAL WINDS IN THE PRODUCTION OF IONOSP--ETC(U)
JUN 78 B D SPRINGER

UNCLASSIFIED 1WW-TN-78-1 NL

1 OF 2
AD A066839



AD-A066839

LEVEL II

0

1WW-TN-78-1

# THE ROLE OF ATMOSPHERIC TIDAL WINDS IN THE PRODUCTION OF IONOSPHERIC SPORADIC-E

Bruce D. Springer, Captain, USAF
Detachment 6, 1st Weather Wing
Hickam AFB, Hawaii 96853

Final Report for Period 1 July 1975 to 30 June 1977

30 June 1978

Approved for public release; distribution unlimited

HEADQUARTERS FIRST WEATHER WING
UNITED STATES AIR FORCE
HICKAM AFB, HAWAII 96853

DDC
RECEIVED
APR 4 1979
D

79 03 09 020

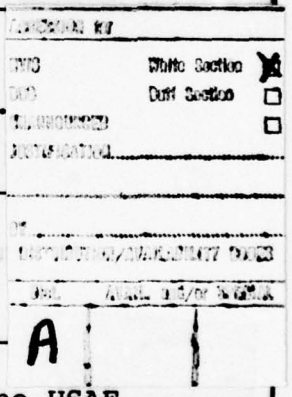
Unclassified

SECURITY CLASSIFICATION OF THIS PAGE (When Data Entered)

| REPORT DOCUMENTATION PAGE | | READ INSTRUCTIONS BEFORE COMPLETING FORM |
|---|---|---|
| 1. REPORT NUMBER<br>1WW-TN-78-1 | 2. GOVT ACCESSION NO. | 3. RECIPIENT'S CATALOG NUMBER |
| 4. TITLE (and Subtitle)<br>THE ROLE OF ATMOSPHERIC TIDAL WINDS IN THE PRODUCTION OF IONOSPHERIC SPORADIC-E | | 5. TYPE OF REPORT & PERIOD COVERED<br>Scientific. Final.<br>1 July 75 to 30 June 77<br>6. PERFORMING ORG. REPORT NUMBER |
| 7. AUTHOR(s)<br>Bruce D. Springer | | 8. CONTRACT OR GRANT NUMBER(s) |
| 9. PERFORMING ORGANIZATION NAME AND ADDRESS<br>Detachment 6, 1st Weather Wing<br>Hickam AFB, HI 96853 | | 10. PROGRAM ELEMENT, PROJECT, TASK AREA & WORK UNIT NUMBERS |
| 11. CONTROLLING OFFICE NAME AND ADDRESS<br>Headquarters First Weather Wing/DON<br>Hickam AFB, HI 96853 | | 12. REPORT DATE<br>30 June 1978<br>13. NUMBER OF PAGES<br>102 |
| 14. MONITORING AGENCY NAME & ADDRESS(if different from Controlling Office) | | 15. SECURITY CLASS. (of this report)<br>Unclassified<br>15a. DECLASSIFICATION/DOWNGRADING SCHEDULE |

16. DISTRIBUTION STATEMENT (of this Report)

Approved for public release; distribution unlimited.




17. DISTRIBUTION STATEMENT (of the abstract entered in Block 20, if different from Report)

18. SUPPLEMENTARY NOTES

This report was prepared under the sponsorship of the USAF Institute of Technology in cooperation with the University of California at Los Angeles.

19. KEY WORDS (Continue on reverse side if necessary and identify by block number)

Ionospheric physics
Sporadic-E
Atmospheric tides

20. ABSTRACT (Continue on reverse side if necessary and identify by block number)

This report summarizes an investigation of the interactions among atmospheric tidal winds, the earth's magnetic field, and metallic ions in the upper atmosphere (90-180 km). The results support the theory that upper atmospheric tidal winds play a critical role in the formation of ionospheric sporadic-E. The contributions of various tidal wind modes are analyzed through the use of extensive computer simulations.

DD FORM 1 JAN 73 1473 EDITION OF 1 NOV 65 IS OBSOLETE

Unclassified

SECURITY CLASSIFICATION OF THIS PAGE (When Data Entered)

**This technical note has been reviewed and is approved for publication.**

**FOR THE COMMANDER:**

Robert W. Smith

TABLE OF CONTENTS


| | | PAGE |
|---|---|---|
| LIST OF FIGURES | | vi |
| LIST OF TABLES | | viii |
| ACKNOWLEDGEMENTS | | ix |
| ABSTRACT | | x |
| I. | INTRODUCTION | 1 |
| II. | ANALYSIS OF WIND-DRIVEN ION MOTION AND CONVERGENCE | 9 |
| III. | THE THEORETICAL ROLE OF ATMOSPHERIC TIDAL WINDS IN THE PRODUCTION AND VERTICAL PROPAGATION OF MID-LATITUDE SPORATIC-E | 24 |
| IV. | COMPARISON OF THEORETICAL RESULTS WITH SPORADIC-E DATA | 56 |
| V. | CONCLUSIONS | 73 |
| APPENDIX 1: | DERIVATION OF THE ION VELOCITY RESULTING FROM MECHANICAL AND ELECTROSTATIC FORCING OF A COLLISIONAL, MAGNETIZED, WEAKLY-IONIZED PLASMA | 75 |
| APPENDIX 2: | DERIVATION OF THE ION VELOCITY DIVERGENCE/CONVERGENCE RESULTING FROM THE MECHANICAL FORCING OF AN IONOSPHERIC PLASMA | 80 |
| APPENDIX 3: | DERIVATION OF THE ION VELOCITY DIVERGENCE/CONVERGENCE RESULTING FROM THE ELECTROSTATIC FORCING OF AN IONOSPHERIC PLASMA | 83 |

TABLE OF CONTENTS (CON'T)


| | | PAGE |
|---|---|---|
| APPENDIX 4: | GRAPHICAL DEPICTION OF THE VERTICAL AND TEMPORAL STRUCTURE OF THE N-S AND E-W COMPONENTS OF THE IMPORTANT E-REGION TIDAL WIND MODES . . . . . | 86 |
| APPENDIX 5: | SCALE ANALYSIS OF VERTICAL ION VELOCITY CONVERGENCE/DIVERGENCE PRODUCED BY REPRESENTATIVE TIDAL WINDS AT $40^{o}$N, $-70^{o}$E . . | 96 |
| BIBLIOGRAPHY . | . . . . . | 100 |

## LIST OF FIGURES


| | | PAGE |
|---|---|---|
| Figure 1 | Night-time sequence of electron density profiles as observed at Wallops Island, Virginia by Smith (1970). | 2 |
| Figure 2 | Geometrical atmospheric factors for selected ion convergence mechanisms. | 18 |
| Figure 3 | Vertical structure of important E-region tidal wind modes. | 31 |
| Figure 4 (a-b) | Latitudinal variation of important E-region tidal wind modes. | 33 |
| Figure 4(a) | Diurnal tidal wind components. | 34 |
| Figure 4(b) | Semidiurnal tidal wind components. | 35 |
| Figure 5 (a-d) | Normalized vertical ion velocities generated at 20°N, -70°E by important E-region tidal wind modes. | 41 |
| Figure 5(a) | (1, 1) mode. | 42 |
| Figure 5(b) | (1, -2) mode. | 43 |
| Figure 5(c) | (2, 2) mode. | 44 |
| Figure 5(d) | (2, 4) mode. | 45 |
| Figure 6 (a-d) | Normalized vertical ion velocity convergence/ divergence generated at 20°N, -70°E by important E-region tidal wind modes. | 46 |
| Figure 6(a) | (1, 1) mode. | 47 |
| Figure 6(b) | (1, -2) mode. | 48 |
| Figure 6(c) | (2, 2) mode. | 49 |
| Figure 6(d) | (2, 4) mode. | 50 |
| Figure 7 | Normalized vertical ion velocity convergence and divergenge produced by a mean, west-to-east, zonal wind. | 53 |

LIST OF FIGURES (CON'T)


| | | PAGE |
|---|---|---|
| Figure 8 | Analysis of sporadic-E virtual height data for Jamaica (20°N, -70°E) for 1-15 March 1965. | 58 |
| Figure 9 | Axes (or planes) of ion divergence corresponding to the axes of ion convergence depicted in Figure 8. | 62 |
| Figure 10 | Analysis of sporadic-E virtual height data for Jamaica (20°N, - 70°E) for 15-31 March 1965. | 64 |
| Figure 11 | Analysis of sporadic-E virtual height data for Akita, Japan (39°N, 140°E) for March 1974. | 67 |
| Figure 12 | Axes (or planes) of ion divergence corresponding to the axes of ion convergence depicted in Figure 11. | 69 |

## LIST OF TABLES


| | | PAGE |
|---|---|---|
| Tables 1-4 | Latitudinal variation of the vertical ion velocity convergence produced by the important E-region tidal wind modes. | 36 |
| Table 1 | (1, 1) mode. | 37 |
| Table 2 | (1, -2) mode. | 38 |
| Table 3 | (2, 2) mode. | 39 |
| Table 4 | (2, 4) mode. | 40 |

## ACKNOWLEDGEMENTS

I wish to personally thank Dr. S.V. Venkateswaran for the guidance, inspiration, and encouragement which he unselfishly offered me during this project.

Recognition should also be extended to Mrs. Beverly Gladstone for preparing the diagrams and Mrs. Grace McMurray for typing the manuscript.

The opportunity to perform this research was afforded me by the USAF Institute of Technology.

## Abstract

Recent theoretical and observational studies have indicated that neutral wind motions in the earth's ionospheric E-region play an important role in the formation and vertical motion of thin, concentrated layers of metallic ions. These metallic ions are commonly called sporadic-E or $E_s$. The formation of sporadic-E layers can be explained by considering a steady-state equilibrium between neutral wind motions and the resultant collisional and geomagnetic forces experienced by the metallic ions in the neutral gas.

The modal oscillations of atmospheric tidal winds generate distinct patterns of ion convergence which control the formation and movement of $E_s$ layers. The interaction of thermally-excited tidal winds and metallic ions in the presence of the earth's magnetic field has been numerically simulated. A comparison of the simulation predictions with observational evidence of sporadic-E occurrences from two widely- separated iononsonde stations indicates that tidal winds play a distinct and predominant role in governing the behavior of mid-latitude $E_s$. The initial results suggest that it may be possible to predict the gross synoptic features of sporadic-E on a global scale.

# I. INTRODUCTION

Sporadic-E, often designated $E_s$, is a term used to describe thin, highly-concentrated, horizontally-stratified layers of ionization which frequently form in the earth's ionospheric E-region (100-150 km). The adjective "sporadic" was originated by early ionospheric researchers who recognized that $E_s$ behavior is not controlled by classical Chapman (1931a, 1931b) photochemical mechanisms.

In general, sporadic-E layers have a common set of characteristics. The vertical thickness of most $E_s$ layers typically ranges between 100 meters and 5 kilometers. Peak ionization concentrations are usually between $10^4$ and $10^6$ electrons $cm^{-3}$. Therefore, the vertically-integrated total electron content for sporadic-E layers spans the range from $10^8$ to $10^{10}$ electrons $cm^{-2}$ (MacLeod, 1975). Since the normal photochemically-produced ionization in the E-region is only on the order of $10^3$-$10^5$ electrons $cm^{-3}$, sporadic-E layers appear as distinct discontinuities in ambient ionization concentration profiles.

Several typical sporadic-E electron concentration profiles are depicted in Figure 1. The series of profiles shown in the figure illustrate several important features which are common to many sporadic-E layers. First, sporadic-E layers tend to form in the upper reaches of the ionospheric E-region, often between 150 and 175 kilometers. Subsequently, they descend to approximately 110 kilometers over a period ranging from 6 to 12 hours. The descent is often accompanied by an enhancement of the ionization concentration of the

layer. In most cases, the increase in the ionization concentration appears to be caused by a vertical compression of the ionized material contained within the layer rather than by the addition of new ionization. Frequently, more than one sporadic-E layer is present in the E-region at the same time (see Figure 1, profile 1). More often than not, the lower $E_s$ layer is a remanent of an older layer which descended from the upper E-region several hours earlier. The tendency for the pattern of descending $E_s$ layers to repeat itself in a cyclical fashion has earned this behavior the name "sequential sporadic-E". To date, the reverse process, i.e., ascending $E_s$ layers, has never been reported. A detailed discussion of sequential sporadic-E, as well as the role played by atmospheric tidal winds in its formation and propagation, will be presented in the subsequent chapters of this report.

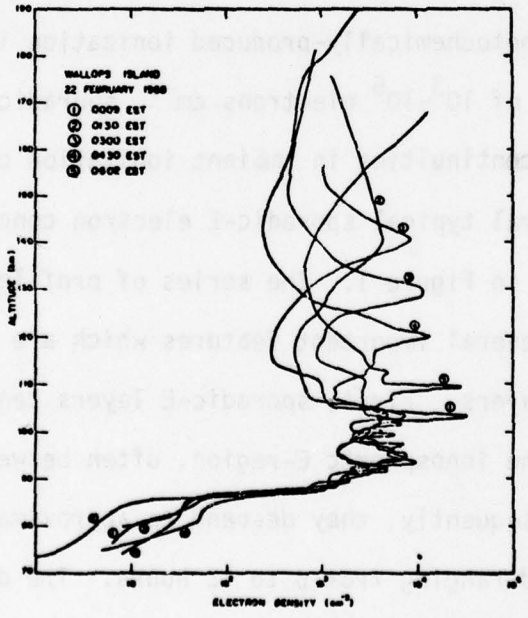



Figure 1. Night-time sequence of electron density profiles as observed at Wallops Island, Virginia, by Smith (1970) (taken from Smith, 1970).

Systematic observations of sporadic-E indicate that the layers often cover large geographical areas. $E_s$ "clouds" spanning horizontal distances of more than 500 kilometers have been measured by sporadic-E ionosonde networks in Europe (Bossy, 1972). Other less reliable measurements (Gersen, 1955) suggest that the horizontal extent of the ionized layers may exceed 1000 kilometers. At the same time, most rocket and ionosonde observations indicate that the ionized material contained within large sporadic-E layers is seldom uniformly distributed. In particular, order of magnitude variations in ionization concentrations of the layers over horizontal and vertical distances of less than 1 kilometer appear to be the rule rather than the exception (Bossy, 1972). Clearly, the extreme inhomogeneties in the distribution of ionization within sporadic-E clouds suggest that complex microscale mechanisms are operating within $E_s$ layers. However, it is not the intent of this paper to examine the small-scale dynamics of sporadic-E layers. Only large, global-scale features will be considered. None-the-less, the complex internal structure of the layers will necessarily complicate comparisons and limit the degree to which large-scale theoretical model predictions can be verified using conventional ionosonde data.

Rocket and ground-based measurements of the chemical composition of sporadic-E layers (Istomin, 1963; Young et. al., 1967); Goldberg et. al., 1973; Philbrick et. al., 1974; Behnke et. al., 1975) all clearly indicate that the layers are largely composed of metallic ions. Although $Fe^+_{56}$, $Si^+_{28}$, and $Mg^+_{24}$ are usually the

predominant ions, other elemental ions, notably $Ni^+_{58}$, $Cr^+_{52}$, $Ca^+_{40}$, and $Na^+_{23}$, have been detected with regularity and considerable certainty. The presence of metallic elements in sporadic-E layers in roughly the same proportions as the elemental composition of meteors suggests that $E_s$ layers are composed of either finely-divided meteoric dust or debris ablated from larger meteors. The outstanding correlation between meteor showers and the intensity and frequency of occurrence of sporadic-E (Appleton et. al., 1947) lends strong additional support to the importance of the role played by meteoric material in the production of sporadic-E.

The presence of metallic elements and compounds in sporadic-E accounts for several unique features of $E_s$ behavior. First, metallic elements and metallic oxide compounds have very low ionization and dissociation potentials (Swider, 1969; Öpik, 1958). Therefore, meteoric material is readily ionized through charge exchange, photoionization or aerodynamic heating processes. Second, once metallic ions are formed, they are lost very slowly. The primary kinetic and chemical loss mechanisms include three body collisions and radiative recombination. Recombination coefficients for either process are typically of the order $10^{-10}$ $cm^3$ $sec^{-1}$. Therefore, lifetimes for the more abundant metallic ions are approximately one day in the lower E-region (Whitehead, 1970).

The unique properties of the ionized metallic elements and compounds found in sporadic-E layers create a regime in which ions are rapidly produced and slowly lost. Consequently, the behavior

of sporadic-E layers in general and metallic ions in particular is largely dominated by wind-driven and electrostatic transport mechanisms while photochemical processes play a secondary role. Accordingly, many ionospheric researchers have attempted to identify the dynamic atmospheric transport mechamisms which can account for the observed formation and vertical propagation of sporadic-E layers.

Presently, it is widely recognized that vertical shears in horizontal ionospheric winds play an important, if not predominant, role in the production of mid-latitude sporadic-E. A large theoretical body of knowledge appropriately termed the "sporadic-E wind-shear theory" has been developed and expanded upon by numerous ionospheric physicists, notably, Dungey (1956, 1959), Whitehead (1961), Smith and Matsushita (1962), MacLeod (1964, 1966, 1968, 1969), MacLeod et. al., (1973), 1975), Keneshea et. al., (1970). Furthermore, the validity and importance of wind-driven ion convergence mechanisms have been repeatedly confirmed by comprehensive theoretical and observational studies (MacLeod 1966, 1975). The success of wind-driven sporadic-E theories in explaining the formation of many $E_s$ layers should not rule out the possibility that other, more complex, sporadic-E mechanisms are not concurrently functioning. Indeed, the inability of the wind-shear theory to explain all the occurrences and features of mid-latitude sporadic-E suggests that all of the important formation mechanisms have not yet been discovered. However, speculation regarding the importance of sporadic-E mechanisms which are driven by forces other than neutral wind motions and their associated dynamo

electric fields is beyond the intended scope of this paper. Furthermore, in order to eliminate the additional E-region complications brought about by energetic particle precipitation at high latitudes and the equatorial electrojet at low latitudes, the subject matter in this thesis will be further confined to the behavior of mid-latitude sporadic-E only.

The specific purpose of this thesis is to examine in detail the role played by atmospheric tidal winds and electrostatic fields in the formation and vertical propagation of ionospheric sporadic-E layers. Although numerically-oriented sporadic-E models have been developed by other researchers (MacLeod, 1975) in order to compare rocket-derived wind measurements with observed occurrences of sporadic-E, there are apparently no published accounts of attempts to numerically model and interpret the behavior of sporadic-E layers produced by atmospheric tidal winds. Therefore, it may be concluded that some of the results presented in this paper are somewhat new and potentially useful in predicting periodic features of mid-latitude sporadic-E layers.

For the reader's benefit, this thesis has been divided into several functionally-independent chapters. The intended objectives of each chapter can be briefly summarized as follows:

Chapter I: Introduction.

a) Define sporadic-E and present a brief outline of its interesting features.

b) Highlight the importance of metallic ions and ionospheric neutral winds in the formation of $E_s$ layers.

Chapter II: Analysis of wind-driven ion motion and convergence.

a) Develop a mathematical analysis of the important wind-driven and electrostatic forcing mechanisms which are capable of producing sporadic-E layers.

b) Offer a detailed interpretation of the physical implications of the analysis.

Chapter III: The theoretical role of tidal winds in the production and vertical propagation of mid-latitude sporadic-E.

a) Discuss how the mathematical analysis presented in Chapter II has been combined with numerical models of the earth's magnetic field, upper air density and thermally-excited atmospheric tides for the purpose of analyzing the influences of both tidal winds and electrostatic fields on the formation and behavior of sporadic-E.

b) Illustrate and discuss the theoretical spatial and temporal sporadic-E patterns which should be produced by the dominant (equinox) atmospheric tidal wind modes.

Chapter IV. Comparison of theoretical results with sporadic-E data.

a) Compare the theoretically-derived, tidally-driven sporadic-E patterns from Chapter III with high-resolution sporadic-E observations from MacDougall (1974a,b) and others.

No detailed review of sporadic-E research is attempted in this paper. However, the reader may find the following references especially useful in this regard:

1) Ionospheric Sporadic-E, Smith and Matsushita, MacMillan Co., N.Y., 1962.

2) Radio Science, v. 7, n. 3, March 1972, Special Issue on Sporadic-E.

3) Radio Science, v. 10, n.3, March, 1975, Special Issue on Sporadic-E.

4) Whitehead, J.D. Production and prediction of sporadic-E, Reviews of Geophysics and Space Physics, 8:65, February 1970.

## II. ANALYSIS OF WIND-DRIVEN ION MOTION AND CONVERGENCE

As discussed in the Introduction to this paper, upper atmospheric neutral winds and long-lived metallic ions have been observed to play an important part in the formation of ionospheric sporadic-E layers. The purpose of this chapter is to mathematically analyze the manner in which atmospheric winds, working in conjunction with magnetic and collisional forces, can compress metallic ions into thin, horizontally-stratified, sporadic-E layers.

In general, the earth's ionospheric E-region can be considered a weakly-ionized and magnetized, collisional plasma. In the central portion of the E-region ($\approx$ 125 km) , the ion gyrofrequency, $\omega_i$ , for moderately heavy ions ($\approx$ 35 a.m.u.) can be shown to be approximately equal to the ion-neutral collision frequency, $\nu_{in}$ . (See Figure 2, profile 1.) In the lower reaches of the E-region ($\approx$ 100 km), $\nu_{in}$ is typically a factor of 10 larger than $\omega_i$ . In the upper extents of the ionospheric E-region ($\approx$ 150 km) just the opposite is true: $\nu_{in}$ is a factor of 10 smaller than $\omega_i$ . Therefore, for the most part, the ions can be considered to be collisionally coupled to neutral (uncharged) atmospheric constituents of the E-region. On the other hand, since the electron gyrofrequency is nearly 1800 times larger than the ion gyrofrequency, the free electrons in the ionospheric E-region are largely decoupled from the neutrals. Therefore, forced, bulk motions of the neutral E-region constituents are quickly

transmitted to the ions, and not the electrons, through collisions.

Accordingly, the wind driven motion of electron-ion pairs in the E-region is largely governed by the vector equation of motion for the ions:

$$m_i n_i \frac{d\underline{V}_i}{dt} = m_i n_i \nu_{in} (\underline{U} - \underline{V}_i) + q_i n_i (\underline{E} + \frac{\underline{V}_i \times \underline{B}}{C}) + m_i n_i \underline{g} - \nabla P_i \qquad (1)$$

where $m_i$: ion mass

$n_i$: ion concentration

$\nu_{in}$: ion-neutral collision frequency

$\underline{U}$: velocity of the neutrals

$\underline{V}_i$: velocity of the ions

$q_i$: ion charge

$\underline{g}$: gravity vector

$\nabla P_i$: ion partial pressure gradient $(\nabla(n_i K T_i))$

The objective at this point is to introduce reasonable assumptions, considerations and observations to simplify the process of solving the equation of motion for the vector ion velocity, $\underline{V}_i$ .

First, it appears reasonable to assume that ion partial pressure gradients in the ionosphere are trivially small in comparison to the other forces in the equation of motion. This is undoubtably the case in classical, non-metallic, Chapman ionospheric layers where photochemical processes clearly predominate over transport mechanisms. The behavior of metallic ion layers is considerably different. The highly-stable chemical characteristics of metallic ions permit wind-driven transport to predominate over the subsidiary role of photochemistry. Therefore, it is possible that ion partial pressure gradients grow to significant proportions in extremely thin (< 100 meters) sporadic-E layers where strong vertical compressional forcing is evident.

Unfortunately, the inclusion of the ion partial pressure gradient term in the equation of motion necessitates the concurrent consideration of the ion continuity equation since:

$$\frac{\partial n_i}{\partial t} = Q_i - L_i + \nabla\cdot(D\nabla n_i - n_i \underline{V}_i) \qquad (2)$$

where: $Q_i$: ion source function

$L_i$: ion loss function

D: ambipolar diffusion coefficient

$n_i, \underline{V}_i$: as previously defined

It is essential that the ion partial pressure gradient term be included in any numerical model written for the expressed purpose of accurately determining absolute metallic ion concentrations in sporadic-E layers. However, since the objective of this thesis is to study only transport mechanisms and not to determine absolute metallic ion concentrations, the ion partial pressure gradient term will be omitted without further consideration. This assumption effectively decouples the equation of motion from the ion continuity equation, eliminates the variable $n_i$ (ion concentration), and significantly simplifies the method of solving the equation of motion for $\underline{V}_i$, the ion velocity.

Next, the force of gravity in the equation of motion, when compared to the collisional and Lorentz forces generated by atmospheric tidal winds ($|\underline{U}| \simeq 10$ to 100 m/s), can be considered insignificant. For example, collisional accelerations (force per unit mass) generated by a 10 m/s difference between the neutral and ion velocities ($|\underline{U} - \underline{V}_i|$) represents a 1000 $m/s^2$ acceleration at 120 kilometers where $\nu_{in} \simeq 100\ sec^{-1}$. Therefore, the omission of gravitational forcing from the equation of motion will result in errors on the order of only 1%. Consequently, the force of gravity can be ignored in the context of the problem under consideration.

Finally, the ion equation of motion can be further simplified by considering only steady-state equilibrium solutions. However, in order to justify the use of steady-state solutions, it is necessary to consider the time required for mechanically-forced ion motions to reach a steady state. This problem has been examined in detail by Piddington (1954). For a mechanically-excited, collisional, magnetic, gas-ion system, Piddington has shown that the time required for the oscillatory ion velocity components to damp one e-fold is of the order $\alpha$ , where:

$$\alpha \equiv \frac{H^2 \sigma_1}{\rho} \tag{3}$$

where H: magnetic field intensity

$\sigma_1$: Hall conductivity ($\approx 10^{-20}$ e.m.u. @ 120 km)

$\rho$: density of the neutrals ($\approx 5 \times 10^{-11}$ gm/cc @ 120 km)

For the middle of the ionospheric E-region ($\approx$ 120 km), $\alpha$ is much less than one inverse second. Therefore, the steady-state ion velocity assumption is an excellent approximation for the diurnal and semidiurnal mechanical forcing motions generated by the predominant atmospheric tidal wind modes.

By combining the simplifying approximations discussed in the previous paragraphs, the ion equation of motion, Equation (1), can be simplified to:

$$m_i \nu_{in} (\underline{U} - \underline{V}_i) + q_i \left( \underline{E} + \frac{\underline{V}_i \times \underline{B}}{C} \right) = 0 \qquad (4)$$

This simplified equation of motion can be rewritten as:

$$\beta_i (\underline{U} - \underline{V}_i) + \underline{\xi} + (\underline{V}_i \times \hat{b}) = 0 \quad , \qquad (5)$$

where: $\beta_i = \nu_{in}/\omega_i$: ratio of ion-neutral collision frequency to ion gyrofrequency

$\hat{b} = \frac{\underline{B}}{|\underline{B}|}$: unit vector parallel to the magnetic field

$\underline{\xi} = \frac{C\underline{E}}{|\underline{B}|}$: reduced electric field (dimensions of velocity)

Basically, this is a statement that a balance exists between the ion-neutral collisional force and the Lorentz force.

Through a series of relatively straight-forward vector manipulations, Equation (5) can be solved for $\underline{V}_i$. The mathematical steps of the derivation are presented in detail in Appendix 1. The essential results are:

$$\underline{V}_i = \left[ \frac{1}{1+\beta_i^2} \right] \left[ \beta_i^2 \underline{U} + \beta_i (\underline{U} \times \hat{b}) + (\underline{U} \cdot \hat{b}) \hat{b} \right]$$

$$+ \left[ \frac{1}{1+\beta_i^2} \right] \left[ \beta_i \underline{\xi} + \underline{\xi} \times \hat{b} + \frac{1}{\beta_i} (\underline{\xi} \cdot \hat{b}) \hat{b} \right] \quad . \qquad (6)$$

Recall that $\underline{V}_i$ in Equation (6) is the steady-state velocity of an ion in a mechanically- and electrostatically-forced, collisional, magnetic, weakly-ionized plasma. In the context of ionospheric sporadic-E, one is interested in determining the circumstances in which the ion velocity converges, since ion velocity convergence corresponds to increasing ionization concentrations. This convergence (negative divergence) can be directly computed from Equation (6).

The complete details of the computations of the ion velocity divergence/convergence from Equation (6) are presented in Appendices 2 and 3. In light of the complexity of the results, the solution will be presented and discussed in two separate parts. The first part will cover wind-driven ion velocity convergence (negative divergence of the first three terms on the right hand side of equation (6)). The second part will consider electrostatically-driven ion velocity convergence (negative divergence of the last three terms on the right hand side of Equation (6)).

Wind-driven ion velocity convergence:

From Appendix 2, the results of the wind-driven ion velocity convergence computations are:

$$-(\nabla\cdot\underline{V}_i)_W = -\nabla\left[\frac{\beta_i^2}{1+\beta_i^2}\right]\cdot\underline{U} - \left[\frac{\beta_i^2}{1+\beta_i^2}\right](\nabla\cdot\underline{U}) - \nabla\left[\frac{\beta_i}{1+\beta_i^2}\right]\cdot(\underline{U}\times\hat{b})$$

$$-\left[\frac{\beta_i}{1+\beta_i^2}\right]\hat{b}\cdot(\nabla\times\underline{U}) - \left[\frac{1}{1+\beta_i^2}\right]\hat{b}\cdot(\hat{b}\cdot\nabla)\underline{U} - (\underline{U}\cdot\hat{b})\,\nabla\left[\frac{1}{1+\beta_i^2}\right]\cdot\hat{b} \qquad (7)$$

Equation (7) implies that six separate wind-driven mechanisms are capable of producing ionospheric sporadic-E. Note that the interpretation of this equation is considerably simplified if the following assumptions are made:

1) Vertical gradients are much larger than horizontal gradients (i.e., $\nabla \simeq \frac{\partial}{\partial z}$ ) .

2) Bulk neutral wind motions are largely horizontal (i.e., $\underline{U}_z \simeq 0$).

If these assumptions are made, it can be deduced from Equation (7) that vertical ion velocity convergence (sporadic-E) should occur under the following circumstances:

1) The cross product of the neutral wind vector with the earth's magnetic field vector has a vertical component (with the appropriate sign). (Term 3, Equation (7)).

2) The neutral wind component perpendicular to the horizontal projection of the earth's magnetic field vector has a vertical shear (of the appropriate sign). (Term 4, Equation (7)).

3) The neutral wind vector component parallel to the horizontal projection of the earth's magnetic field has a vertical shear (of the appropriate sign). (Term 5, Equation (7)).

4) The neutral wind has a vector component parallel to the horizontal projection of the earth's magnetic field. (Term 6, Equation (7)).

Under the imposed assumptions ($\nabla = \frac{\partial}{\partial z}$ , $\underline{U}_z = 0$) , the first and second terms in Equation (6) are incapable of generating vertical ion velocity convergence.

It is interesting to note that the four wind-driven $E_s$ production mechanisms can be divided into two classes. The first class consists of sporadic-E production mechanisms which depend on vertical shears in the horizontal neutral winds (terms 4 and 5, Equation (7)). Henceforth, these terms will be referred to as the "wind-shear $E_s$ mechanisms". The second class contains the vertical ion velocity convergence mechanisms which function because of vertical gradients in $\beta_i$, the ratio of the ion-neutral collision frequency to the ion gyrofrequency (terms 3 and 6, Equation (7)). These two terms will be designated the "non-shear $E_s$ mechanisms".

It is important to note that two of the $E_s$ mechanisms operate only when the neutral wind has a component <u>perpendicular</u> to the horizontal projection of the earth's magnetic field (terms 3 and 4, Equation (7)). In contrast, the other two mechanisms (terms 5 and 6, Equation (7)) function only when the neutral wind has a component <u>parallel</u> to the horizontal projection of the earth's magnetic field.

The geometrical atmospheric factors for the various terms in Equation (7) have been numerically computed using Jacchia's (1971) neutral density model and Chapman's (1956) ion-neutral collision frequency model. The computations were based on a magnetic field intensity of .30 Gauss and an ion mass of 24 a.m.u. ($Mg^+_{24}$). The results of the computations are depicted in Figure 2. Profiles 3, 4, 5, and 6 illustrate how the geometrical atmospheric factors for terms 3, 4, 5, and 6 (respectively) in Equation (7) vary with altitude.

Figure 2 Geometrical atmospheric factors for selected ion convergence mechanisms.

Legend:

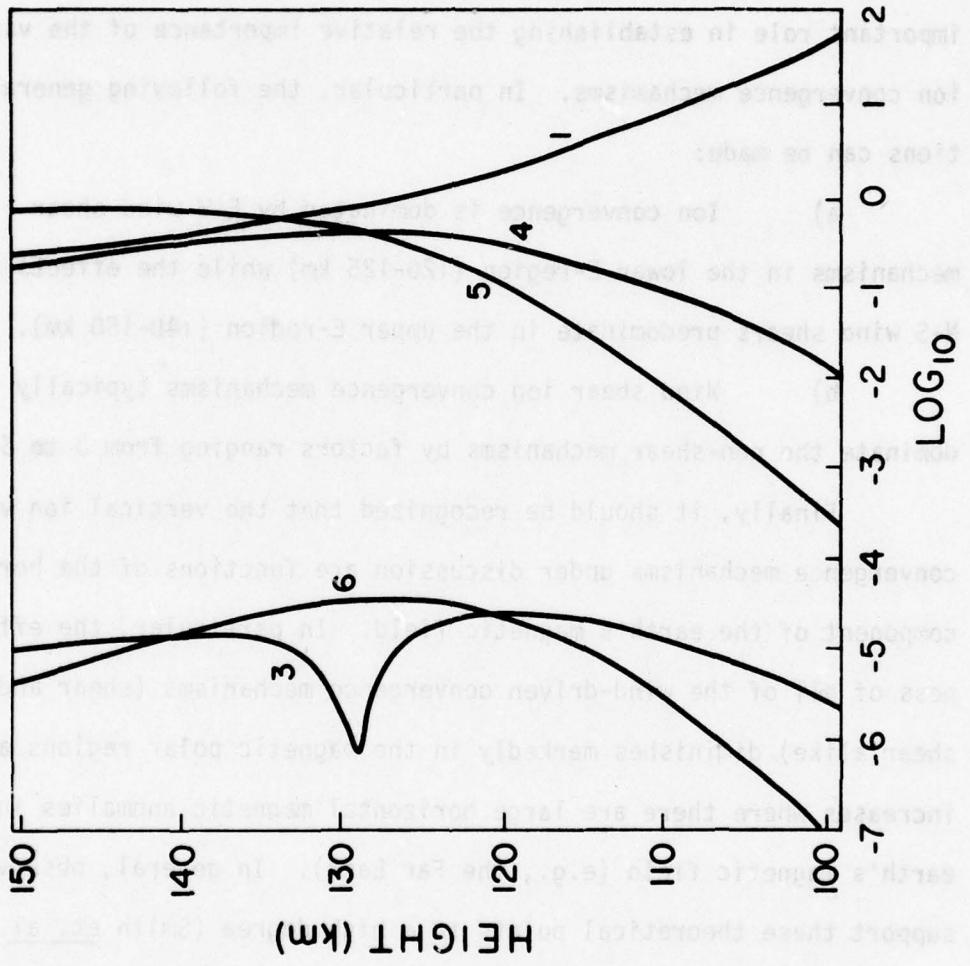
1: $\beta_i \equiv \frac{\nu_{in}}{\omega_i}$

3: $\left|\frac{\partial}{\partial z}\left(\frac{\beta_i}{1+\beta_i^2}\right)\right|$ $m^{-1}$

4: $\frac{\beta_i}{1+\beta_i^2}$

5: $\frac{1}{1+\beta_i^2}$

6. $\left|\frac{\partial}{\partial z}\left(\frac{1}{1+\beta_i^2}\right)\right|$ $m^{-1}$


HEIGHT (km)
150
140
130
120
110
100
LOG10
2
1
0
-1
-2
-3
-4
-5
-6
-7
1
4
5
6
3

A scale analysis of the important wind (and electrostatic) ion convergence mechanisms has been performed using the coefficients from Figure 2 in conjunction with representative ionospheric (tidal) winds. The detailed results are presented in Appendix 5. The results confirm the fact that atmospheric geometric effects ($\beta_i$) play an important role in establishing the relative importance of the various ion convergence mechamisms. In particular, the following generalizations can be made:

a) Ion convergence is dominated by E-W wind shear mechanisms in the lower E-region (120-125 km) while the effects of N-S wind shears predominate in the upper E-region (140-150 km).

b) Wind shear ion convergence mechanisms typically dominate the non-shear mechanisms by factors ranging from 3 to 5.

Finally, it should be recognized that the vertical ion velocity convergence mechanisms under discussion are functions of the horizontal component of the earth's magnetic field. In particular, the effectiveness of all of the wind-driven convergence mechanisms (shear and non-shear alike) diminishes markedly in the magnetic polar regions and increases where there are large horizontal magnetic anomalies in the earth's magnetic field (e.g., the Far East). In general, observations support these theoretical points to a high degree (Smith et. al., 1960). A more detailed analysis of the role played by magnetic field variations in sporadic-E formation will be considered in the next chapter.

Electrostatically-driven ion velocity convergence:

The ion velocity convergence (negative divergence) produced by electrostatic fields can be computed by taking the convergence of the last three terms of the right-hand side of Equation (6). The details of the derivation are presented in Appendix 3. The essential results are:

$$-(\nabla\cdot\underline{V}_i)_E = -\nabla\left[\frac{\beta_i}{1+\beta_i^2}\right]\cdot\underline{\xi} - \left[\frac{\beta_i}{1+\beta_i^2}\right](\nabla\cdot\underline{\xi}) - \nabla\left[\frac{1}{1+\beta_i^2}\right]\cdot(\underline{\xi}\times\hat{b})$$

$$-\left[\frac{1}{1+\beta_i^2}\right]\hat{b}\cdot(\nabla\times\underline{\xi}) - \left[\frac{1}{\beta_i(1+\beta_i^2)}\right]\hat{b}\cdot((\hat{b}\cdot\nabla)\underline{\xi})$$

$$-(\underline{\xi}\cdot\hat{b})\,\nabla\left[\frac{1}{\beta_i(1+\beta_i^2)}\right]\cdot\hat{b} \quad . \qquad (8)$$

Equation (8) implies that six separate electrostatically-driven mechanisms are capable of producing ionospheric sporadic-E. The interpretation of Equation (8) is simplified if the following assumptions are made:

1) Ionospheric plasmas are neutral, i.e., net charge is zero ($\nabla \cdot \underline{\xi} = 0$).

2) Time-dependent, magnetic field variations are small. $\nabla \times \underline{\xi} \simeq 0$ .

3) Field-aligned electric fields are small ($\underline{\xi} \cdot \hat{b} \simeq 0$).

4) Vertical gradients are much larger than horizontal gradients ($\nabla \simeq \frac{\partial}{\partial z}$).

If these assumptions are made, Equation (8) implies that vertical ion velocity convergence (sporadic-E) should occur under the following circumstances:

1) $\underline{\xi}$ has a vertical component (pointing in the proper direction). (Term 1, Equation (8)).

2) The cross-product between $\underline{\xi}$ and the earth's magnetic field vector has a vertical component (pointing in the proper direction). (Term 3, Equation (8)). This is the familiar ExB drift.

Under the imposed assumptions, the remaining terms in Equation (8) (terms 2, 4, 5, and 6) are incapable of generating vertical ion velocity convergences.

A scale analysis of the important electrostatic (and wind-driven) ion convergence mechanisms is presented in Appendix 5. The results show that electrostatically-driven ion convergence is typically an order of magnitude smaller than wind-driven convergence.

Therefore, it appears that electrostatic fields play a subordinate role to the wind-driven convergence mechanisms. This conclusion is supported by the work of MacLeod (1964, 1975) and others. Therefore, the remainder of this thesis will concentrate on the major role played by neutral wind motions in the production of sporadic-E.

Summary

In this chapter, the velocity of an ion in a wind-driven, collisional, magnetized, weakly-ionized plasma was computed. In turn, this result was used to compute the ion's vertical velocity convergence. Subsequent analysis showed that four wind-driven ion convergence mechanisms are capable of producing sufficient vertical ion convergence to produce sporadic-E layers. Additionally, it was shown that two electrostatically-driven convergence mechanisms can also contribute to ion convergence. These mathematical results will be used in the next chapter to compute the sporadic-E patterns which should be produced by atmospheric tidal winds.

## III. THE THEORETICAL ROLE OF ATMOSPHERIC TIDAL WINDS IN THE PRODUCTION AND VERTICAL PROPAGATION OF MID-LADITUDE SPORADIC-E

The purpose of the previous chapter was to derive the equations which describe the motions and convergence of metallic ions in the ionospheric E-region. This chapter will describe how these equations have been incorporated into a computer model of the earth's ionosphere for the purpose of studying the spatial and temporal patterns of sporadic-E produced by various atmospheric tidal wind modes.

Since sporadic-E is produced largely by the vertical convergence of metallic ions, the mathematical modelling of $E_s$ layers is greatly simplified if the analysis is restricted to motions and convergence along the vertical coordinate only. Therefore, the numerical sporadic-E model which will be presented in this chapter is purely one-dimensional. For the one-dimensional case, the wind-driven, vertical component of the ion velocity equation can be written as:

$$\underline{V}_{iz} = \left[\frac{\beta_i}{1+\beta_i^2}\right](\underline{U}_x\hat{b}_y - \underline{U}_y\hat{b}_x) + \left[\frac{1}{1+\beta_i^2}\right](\underline{U}_x\hat{b}_x + \underline{U}_y\hat{b}_y)\hat{b}_z \qquad (9)$$

Next, the vertical ion velocity convergence can be readily computed from Equation (9):

$$-\frac{\partial \underline{V}_{iz}}{\partial z} = -\left(\frac{\beta_i}{1+\beta_i^2}\right)\left(\frac{\partial \underline{U}_x}{\partial z}\hat{b}_y - \frac{\partial \underline{U}_y}{\partial z}\hat{b}_x\right) - \left(\frac{1}{1+\beta_i^2}\right)\left(\frac{\partial \underline{U}_x}{\partial z}\hat{b}_x + \frac{\partial \underline{U}_y}{\partial z}\hat{b}_y\right)\hat{b}_z$$

$$+ (\underline{U}_x\hat{b}_y - \underline{U}_y\hat{b}_x)\frac{\partial}{\partial z}\left(\frac{\beta_i}{1+\beta_i^2}\right) - (\underline{U}_x\hat{b}_x + \underline{U}_y\hat{b}_y)\hat{b}_z\frac{\partial}{\partial z}\left(\frac{1}{1+\beta_i^2}\right) \qquad (10)$$

In order to numerically simulate the behavior of sporadic-E, mathematical parameterizations for all of the variables in Equations (9) and (10) must be specified. The parameterizations used in the sporadic-E model which has been developed can be summarized as follows:

a) Magnetic field:

The magnetic field components were derived from the International Geomagnetic Reference Field (IGRF 1965.0). Specifically, the three components of the earth's magnetic field were computed in geomagnetic coordinates from a series of spherical harmonics and their derivatives in geocentric coordinates. The expressions used for each of the components ( x: east; y: north; z: vertical) are as follows:

$$B_x = -\frac{1}{r \sin\theta}\frac{\partial V}{\partial \lambda} = \sum_{n=1}^{8}\sum_{m=0}^{m}\left(\frac{a}{a+h}\right)^{n+2}\frac{(-m)}{\sin\theta}$$

$$\cdot\left[-g_n^m \sin(m\lambda) + h_n^m \cos(m\lambda)\right] P_n^m(\cos\theta)$$

$$B_y = \frac{1}{r}\frac{\partial V}{\partial \theta}\sum_{n=1}^{8}\sum_{m=0}^{n}\left(\frac{a}{a+h}\right)^{n+2}$$

$$\cdot\left[g_n^m \cos(m\lambda) + h_n^m \sin(m\lambda)\right]\frac{d}{d\theta}P_n^m(\cos\theta)$$

$$B_z = -\frac{\partial V}{\partial r} = \sum_{n=1}^{8}\sum_{m=0}^{n}(n+1)\left(\frac{a}{a+h}\right)^{n+2}$$

$$\cdot\left[g_n^m \cos(m\lambda) + h_n^m \sin(m\lambda)\right] P_n^m(\cos\theta)$$

where

$$V = a\sum_{n=1}^{8}\sum_{m=0}^{n}\left(\frac{a}{a+h}\right)^{n+1} \quad \text{(magnetic potential)}$$

$$\cdot\left[g_n^m \cos(m\lambda) + h_n^m \sin(m\lambda)\right] P_n^m(\cos\theta)$$

$P_n^m$ (cos $\theta$): Associated Legendre function

a: radius of the earth (6371.2 km)

h: height above earth

$\theta$: geomagnetic colatitude

$h_n^m$, $g_n^m$: IGRF 1965.0 coefficients

b) Ion-neutral collision frequency

The ion-neutral collision frequency, i.e., $\nu_{in}$ occurring in parameter $\beta_i$, was derived from Chapman (1956). In particular, Chapman has shown that $\nu_{in}$ can be represented by the following equation:

$$\nu_{in} = 2.6 \times 10^{-9} \; M^{-1/2} \; N \; sec^{-1}$$

where

M: ion mass (a.m.u.)

N: concentration of neutrals (c.g.s. units)

c) Neutral atmosphere:

An atmospheric neutral density model must be used in the process of computing absolute values for the ion-neutral collision frequency. Jacchia's (1971) neutral atmospheric density model was selected for this purpose. Jacchia's particular parameterization of the atmosphere includes empirical correlations between neutral density and numerous geophysical variables. The results presented in this chapter were computed using the following values for these geophysical parameters:

| | |
|---|---|
| $K_p$ index: | + 1 |
| Mean Julian Day: | 42495.0 (Vernal equinox, 1975) |
| 10.7 cm solar flux: | $136 \times 10^{-22}$ watts $m^{-2}$ $H_z^{-1}$ |
| Averaged solar flux: | $155 \times 10^{-22}$ watts $m^{-2}$ $H_z^{-1}$ |
| Solar declination: | $0^o$ |

c) Atmospheric tidal winds:

An important aspect of developing a numerical model to study the effects of tidal winds on sporadic-E is the formulation of a tidal wind model. Classical solutions to the problem of computing thermally-forced tidal wind motions have been presented by Wilkes (1949), Siebert (1961), and Lindzen and Chapman (1969).

However, these solutions do not include the dissipative forces which are particularly important in the ionospheric E-region.

According to dissipationless tidal theory, the amplitude of tidal winds increases exponentially with altitude. Clearly, this is unrealistic.

A more satisfactory solution for the height variation of the tidal winds has been derived by Richmond (1971) by including the dissipative effects of the Lorentz force, molecular viscosity and heat conductivity. The height structure of the winds used in the wind-driven sporadic-E model are those given by Richmond.

In the following sections of this chapter, the theoretical temporal and spatial sporadic-E patterns generated by Richmond's tidal winds will be presented and analyzed. Each of the distinct tidal wind modes which will be considered in this study will be designated by two letters: n and m . The letter n represents the longitudinal wave number (or the temporal periodicity) of the mode while the letter m describes the latitudinal structure. In particular, the following standard conventions have been adopted for n and m in this paper.

| | |
|---|---|
| n = 1: | diurnal mode |
| n = 2: | semidiurnal mode |
| m positive: | vertically propagating mode |
| m negative: | evanescent mode |
| m even: | symmetrical with respect to the geographic equator |
| m odd: | asymmetrical with respect to the geographic equator |

In general, the various tidal wind modes which occur in the atmosphere result from the thermal forcing produced by IR absorption by water vapor in the troposphere and UV absorption by ozone in the stratosphere. However, the excitation and propagation of tides is a complex problem. Theoretical and observational studies indicate that the (1, 1) and (1, -2) diurnal modes and the (2, 2) and (2, 4) semidiurnal modes are the important modes in the E-region. Therefore, this thesis will concentrate on analyzing the spatial and temporal behavior of the sporadic-E patterns produced by these particular modes.

The vertical and latitudinal structure for each of the aforementioned tidal wind modes is illustrated in Figures 3 and 4 respectively. For the sake of comparison, the amplitude of each mode has been normalized to one. The phase profiles depicted in Figure 3 are a measure of how the polarization of the vertically propagating wave varies with altitude. A graphical depiction of the east-west and north-south components of the important tidal wind modes is presented in Appendix 4.

Using Richmond's (1971) ionospheric tidal wind model, the vertical ion velocity and vertical ion velocity convergence patterns for the (1, 1), (1, -2), (2, 2), and (2, 4) modes have been computed for latitudes between $10^{o}$ N and $70^{o}$N. A summary of the analysis of the results for $10^{o}$ latitude increments along the zero magnetic meridian ($\approx 70^{o}$ E longitude) is presented in Tables 1 through 4. Analysis along the zero magnetic meridian was chosen to eliminate the necessity of considering variations in the sporadic-E patterns

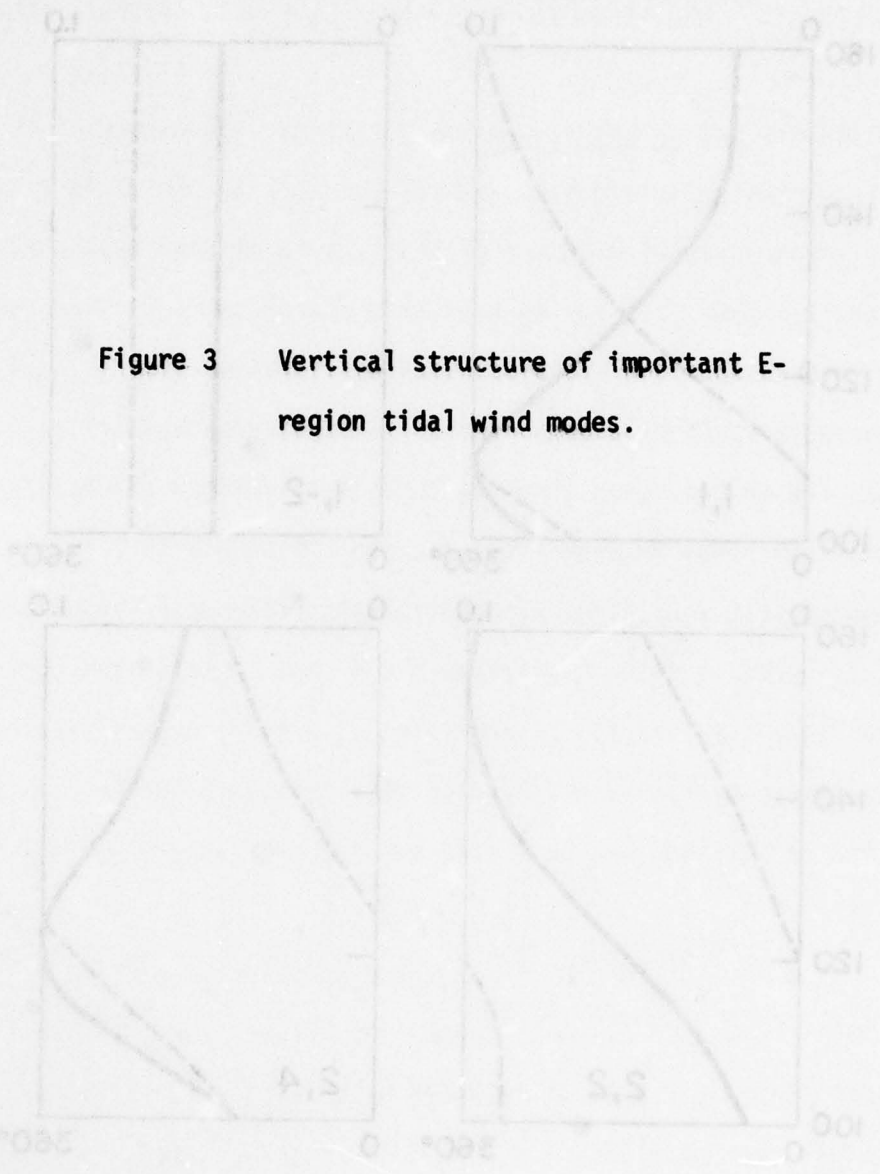
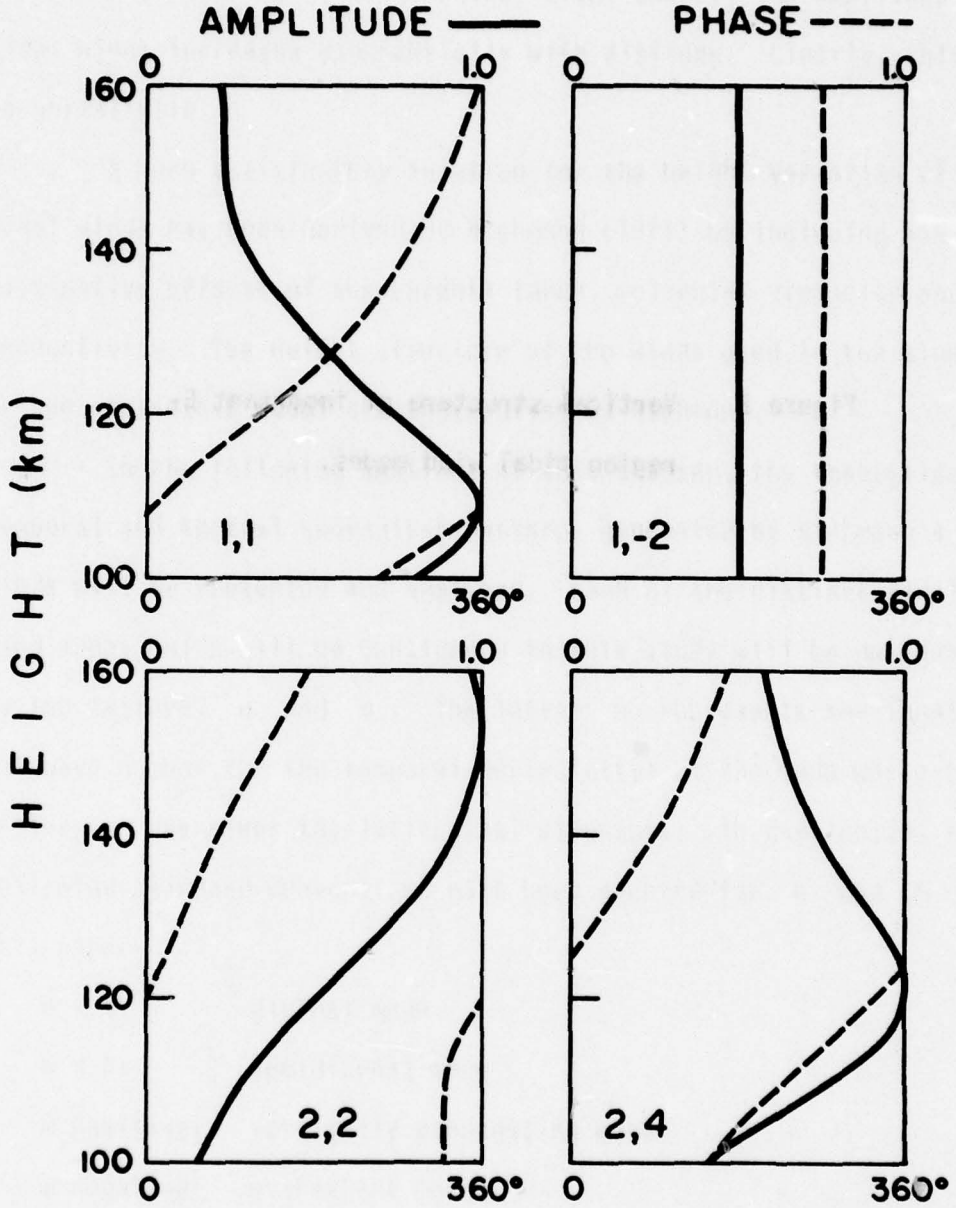


Figure 3 Vertical structure of important E-region tidal wind modes.


AMPLITUDE
PHASE
HEIGHT (km)
160
140
120
100
0
1.0
360°
1,1
1,-2
2,2
2,4

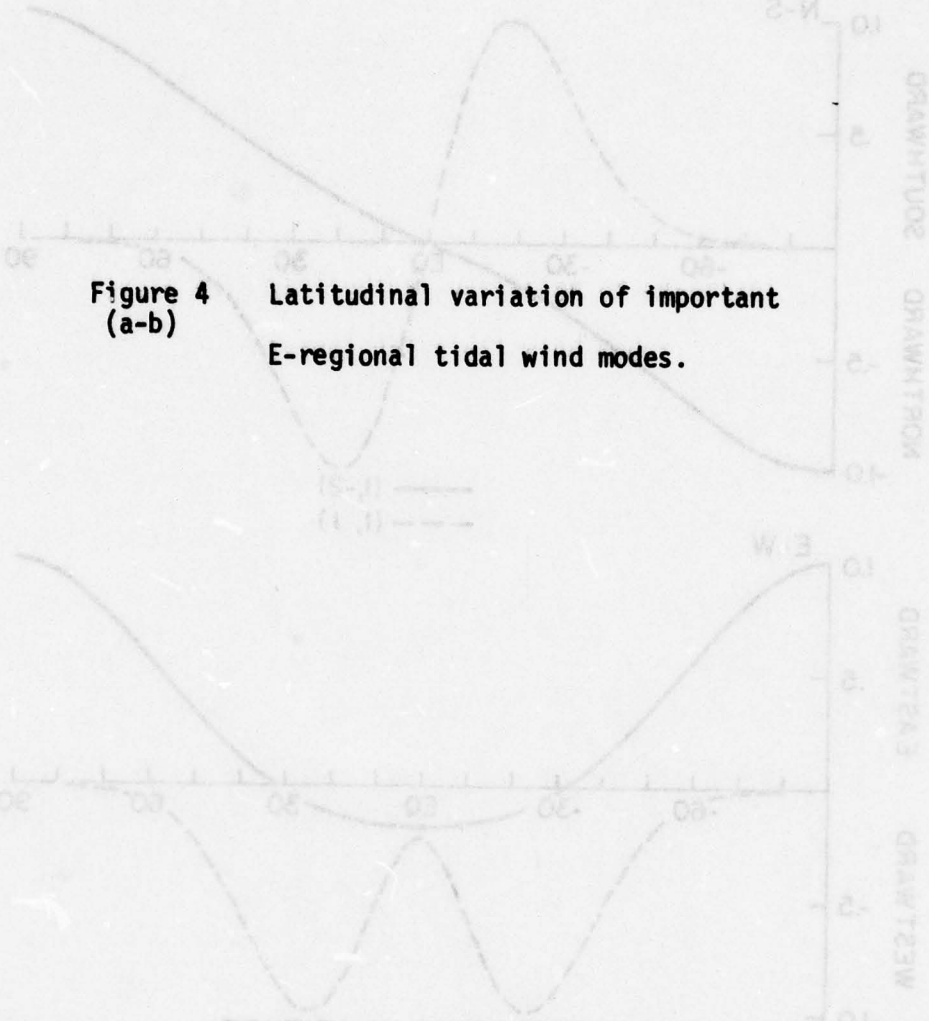


Figure 4 (a-b) Latitudinal variation of important E-regional tidal wind modes.

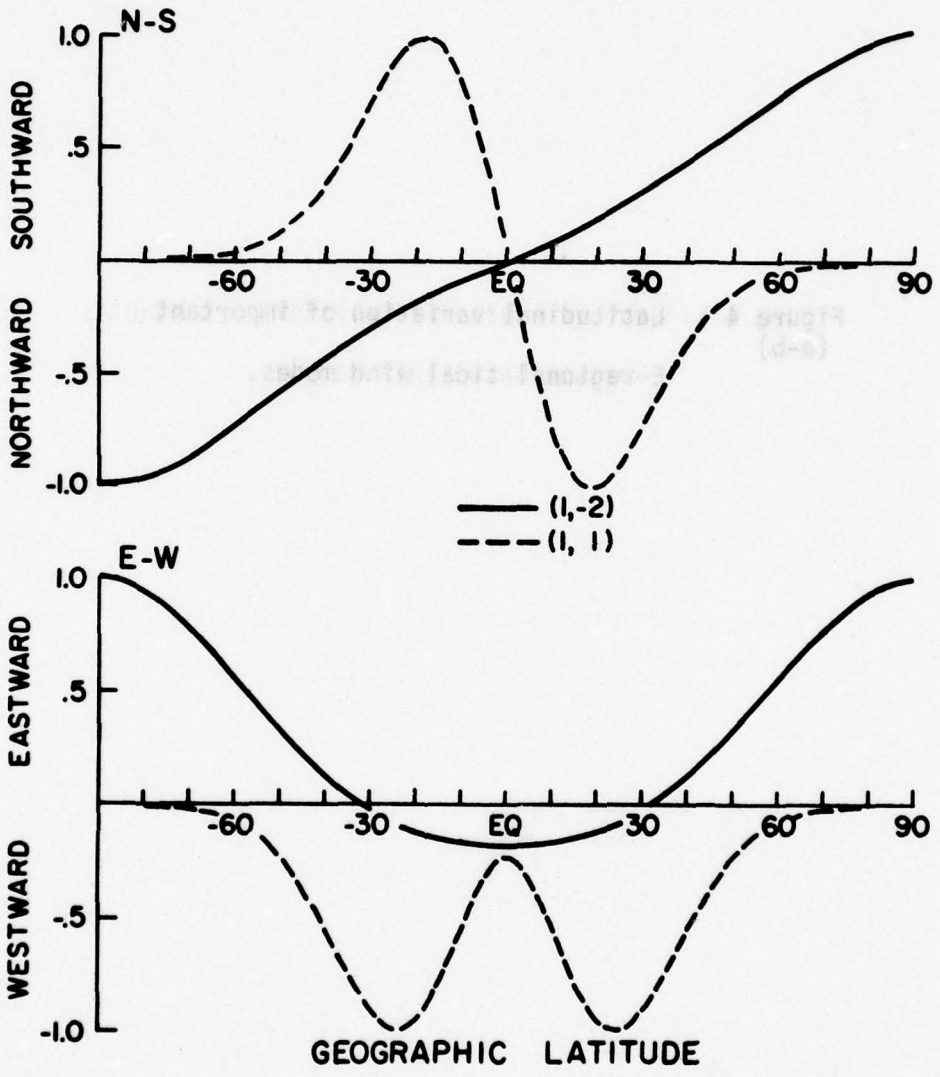



Figure 4(a) Diurnal tidal wind components

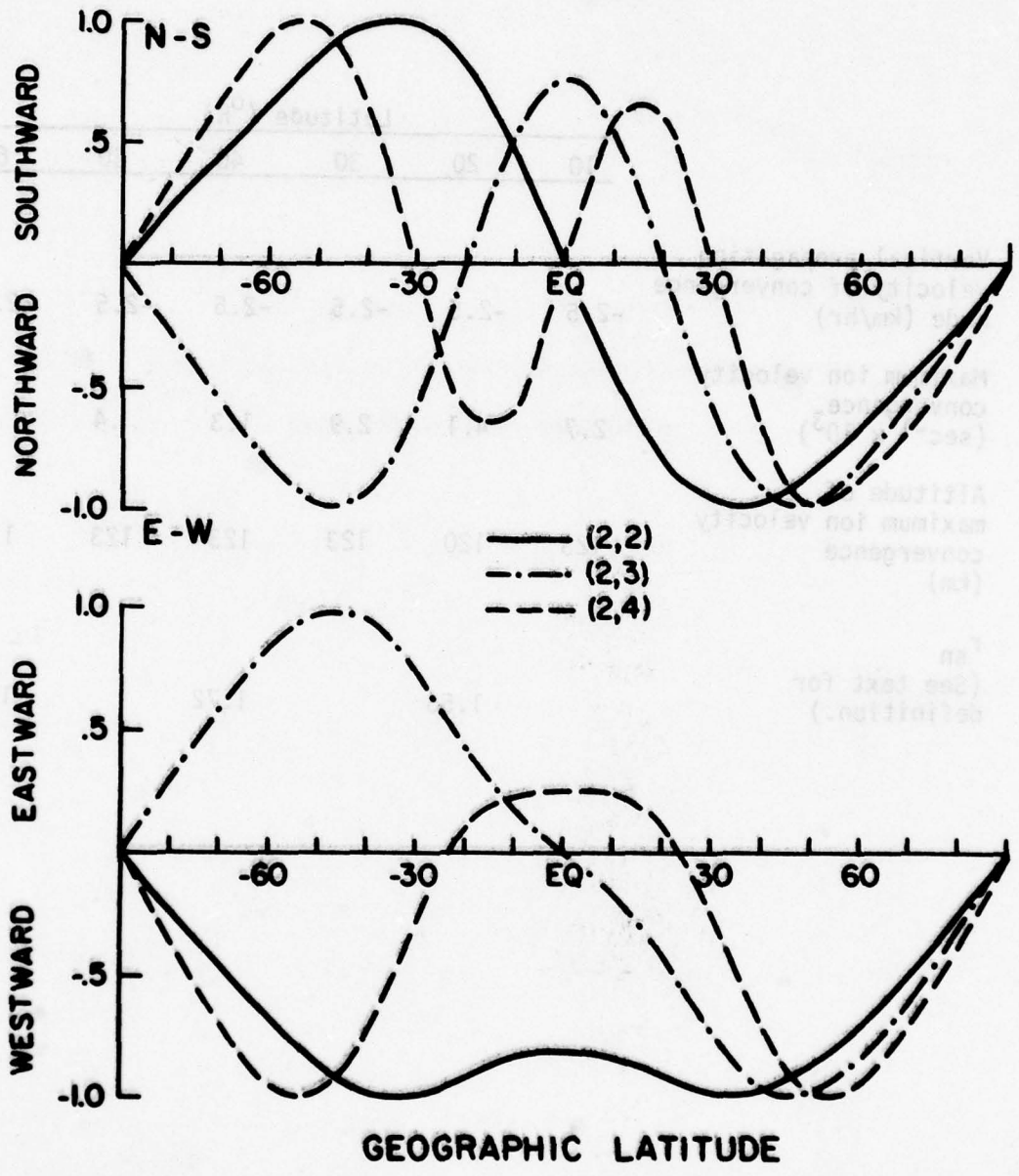



Figure 4(b) Semidiurnal tidal wind components

Table 1: Latitudinal variation of the vertical ion velocity convergence produced by the (1, 1) tidal wind. (Computations based on a maximum N-S wind component of 10 m/s at $20^{o}$ N.)

| | Latitude ($^{o}$N) | | | | | |
|---|---|---|---|---|---|---|
| | 10 | 20 | 30 | 40 | 50 | 60 |
| Vertical propagation velocity of convergence node (km/hr) | -2.5 | -2.5 | -2.5 | -2.5 | -2.5 | -2.5 |
| Maximum ion velocity convergence, ($sec^{-1} \times 10^{3}$) | 2.7 | 4.1 | 2.9 | 1.3 | .4 | .06 |
| Altitude of maximum ion velocity convergence (km) | 123 | 120 | 123 | 123 | 123 | 119 |
| $r_{sn}$ (See text for definition.) | | 1.56 | | 1.72 | | 1.85 |

Table 2: Latitudinal variation of the vertical ion velocity convergence produced by the (1, -2) tidal wind. (Computations based on a maximum N-S wind component of 10 m/s at 20° N.)

| | Latitude (°N) | | | | | |
|---|---|---|---|---|---|---|
| | 10 | 20 | 30 | 40 | 50 | 60 |
| Vertical propagation velocity of convergence node (km/hr) | 0 | -2.5 | 0 | +1.0 | +2.5 | +2.5 |
| Maximum ion velocity convergence ($sec^{-1} \times 10^3$) | .21 | .23 | .34 | .36 | .34 | .22 |
| Altitude of maximum ion velocity convergence (km) | 120 | 125 | 125 | 125 | 125 | 125 |
| $r_{sn}$ (See text for definition.) | 0 | 0 | 0 | 0 | 0 | 0 |

Table 3: Latitudinal variation of the vertical ion velocity convergence produced by the (2, 2) tidal wind. (Computations based on a maximum N-S wind component of 10 m/s at 20° N.)

| | Latitude (°N) | | | | | |
|---|---|---|---|---|---|---|
| | 10 | 20 | 30 | 40 | 50 | 60 |
| Vertical propagation velocity of convergence node (km/hr) | -10 | -10 | -10 | -10 | -10 | -10 |
| Maximum ion velocity convergence ($sec^{-1} \times 10^3$) | 3.2 | 5.8 | 5.2 | 4.2 | 2.5 | 1.0 |
| Altitude of maximum ion velocity convergence (km) | 141 | 142 | 143 | 143 | 143 | 143 |
| $r_{sn}$ (See text for definition.) | | 2.94 | | 2.94 | | 3.13 |

Table 4: Latitudinal variation of the vertical ion velocity convergence produced by the (2, 4) tidal wind. (Computations based on a maximum N-S wind component of 10 m/s at 20° N.)

| | Latitude (°N) | | | | | |
|---|---|---|---|---|---|---|
| | 10 | 20 | 30 | 40 | 50 | 60 |
| Vertical propagation velocity of convergence node (km/hr) | -5 | -5 | -5 | -5 | -5 | -5 |
| Maximum ion velocity convergence ($sec^{-1} \times 10^3$) | 3.5 | 3.7 | 1.1 | 2.9 | 2.7 | 1.3 |
| Altitude of maximum ion velocity convergence (km) | 141 | 142 | 122 | 130 | 137 | 141 |
| $r_{sn}$ (See text for definition.) | | 1.69 | | 1.79 | | 1.59 |

produced by magnetic declination effects. To facilitate the comparison of the sporadic-E patterns, the computations for each mode were made using a maximum southward wind component of 10 m/s at $20^{o}$ N. In Tables 1 through 4, the parameter $r_{sn}$ is computed by dividing the maximum value of shear-produced ion convergence by the maximum convergence produced by non-shear mechanisms.

The normalized temporal and height variations in the vertical ion velocity produced by each tidal wind mode at $20^{o}$ N, $-70^{o}$ E are presented in graphical form in Figures 5(a) through 5(d). The numbers in the figures represent vertical (upward) ion velocities. The letters represent vertical (downward) ion velocities. The number 5 and the letter E signify the absolute maximum normalized ion velocities.

Figures 6(a) through 6(d) illustrate the normalized vertical ion velocity convergence patterns corresponding to the data in Figures 5(a) through 5(d). The letter E in the diagrams represents the maximum normalized vertical ion velocity convergence while the number 5 indicates the maximum ion velocity divergence. Sporadic-E should form in those areas where the ion convergence is the greatest.

The particular phases (i.e., local times) selected for the generation of Figures 5 and 6 were specifically chosen to facilitate the comparison of these figures with sporadic-E observations presented in the next chapter.

Based on the information presented in Figures 6(a) through 6(d) and Tables 1 through 4, the following observations regarding the latitudinal behavior of tidally-driven sporatic-E can be made:

Figure 5 (a-d) Normalized vertical ion velocities generated at $20^{o}N$, $-70^{o}E$ by important E-region tidal wind modes.

Legend: Numbers represent vertically upward ion motion.

Letters represent vertically downward ion motion.

Note: Scaling is linear.

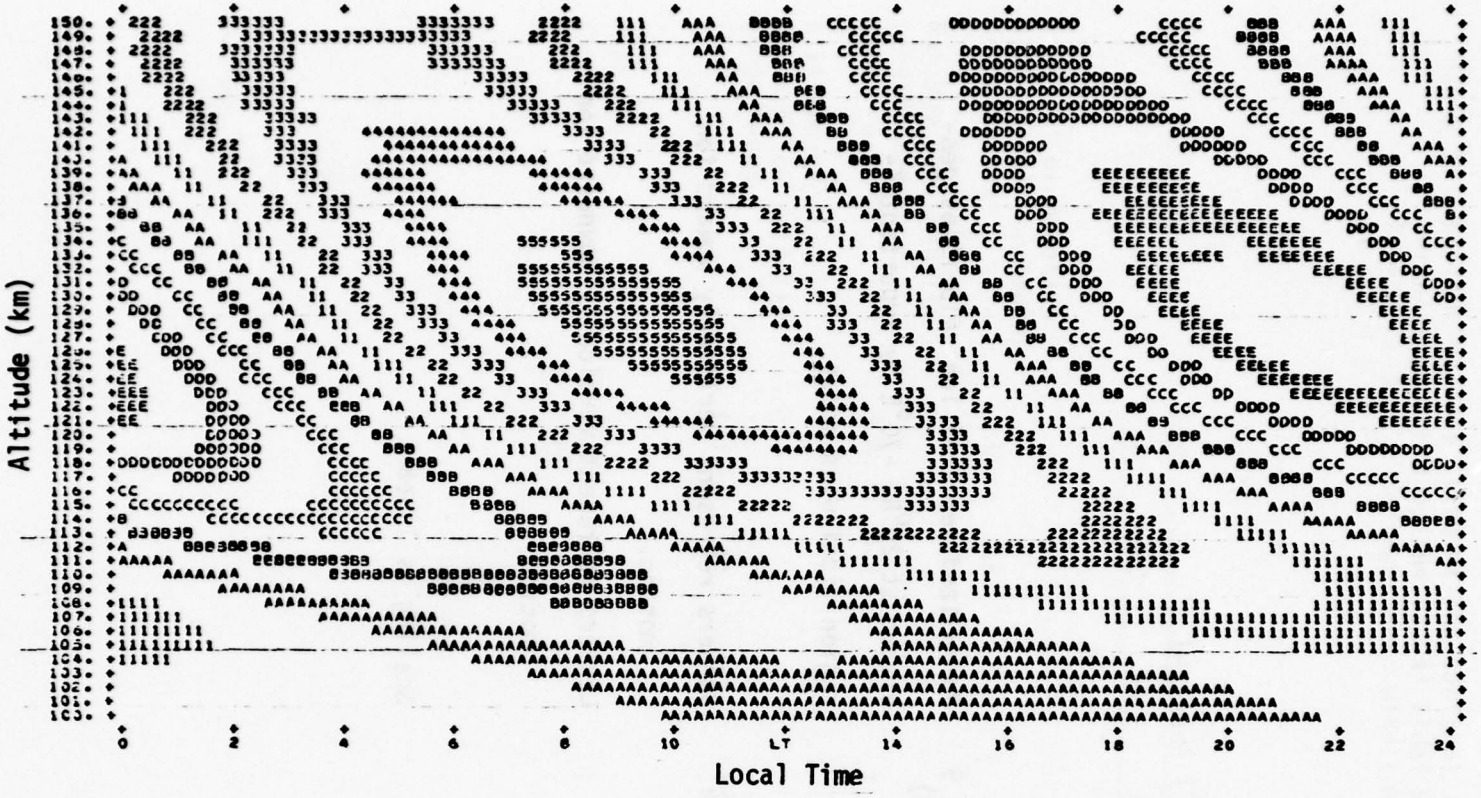



Figure 5(a) (1, 1) mode.

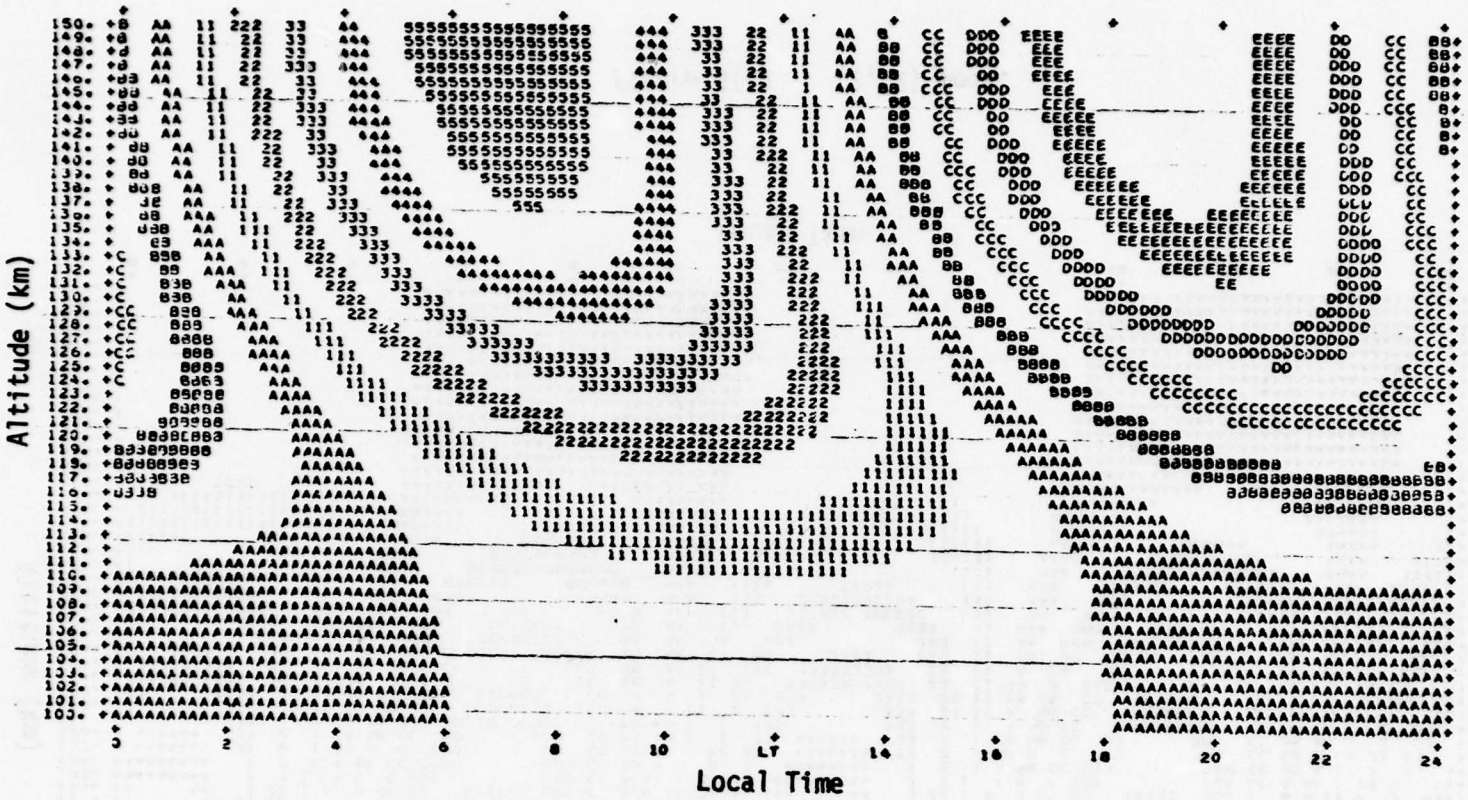



Figure 5(b) (1, -2) mode.

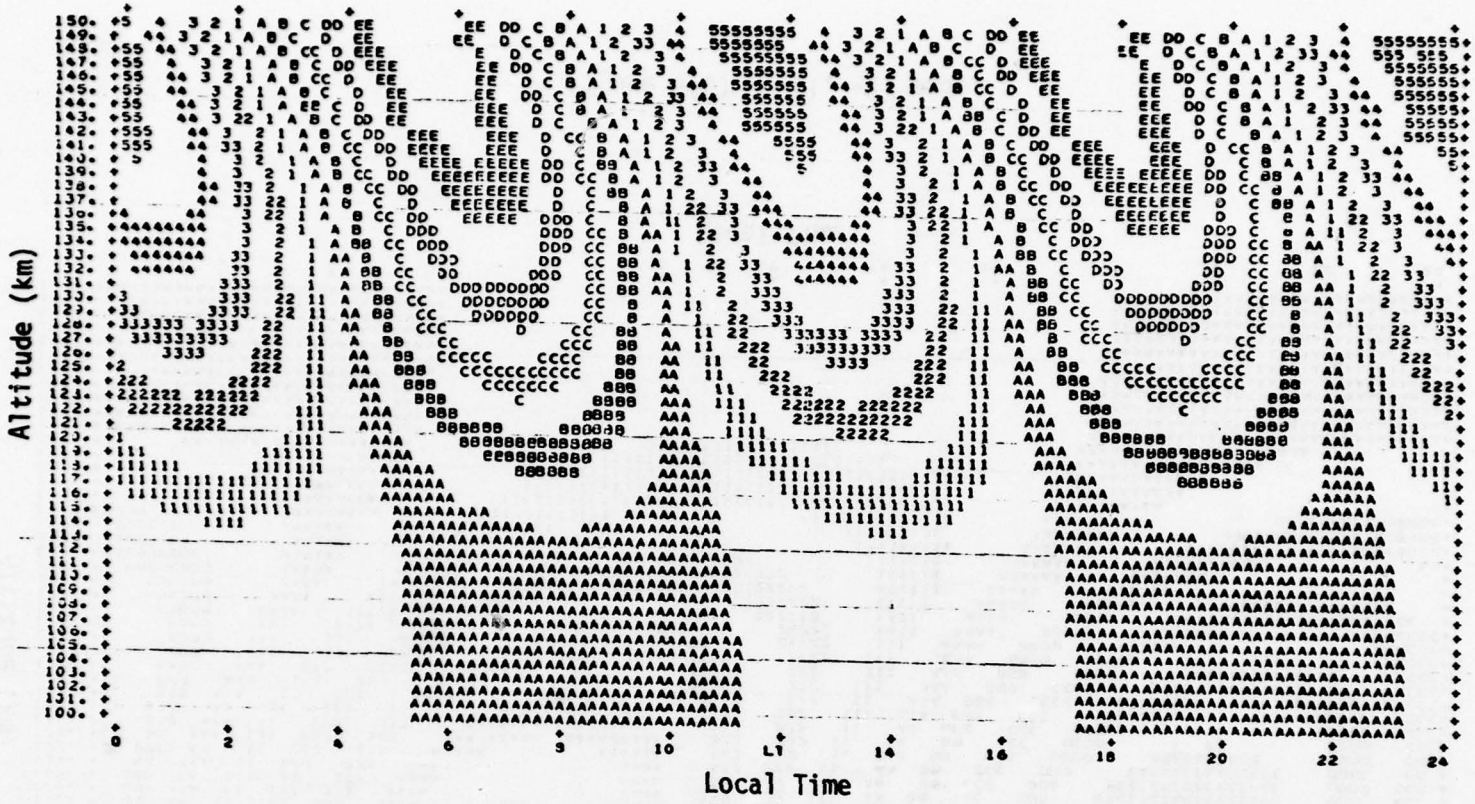



Figure 5(c) (2, 2) mode.

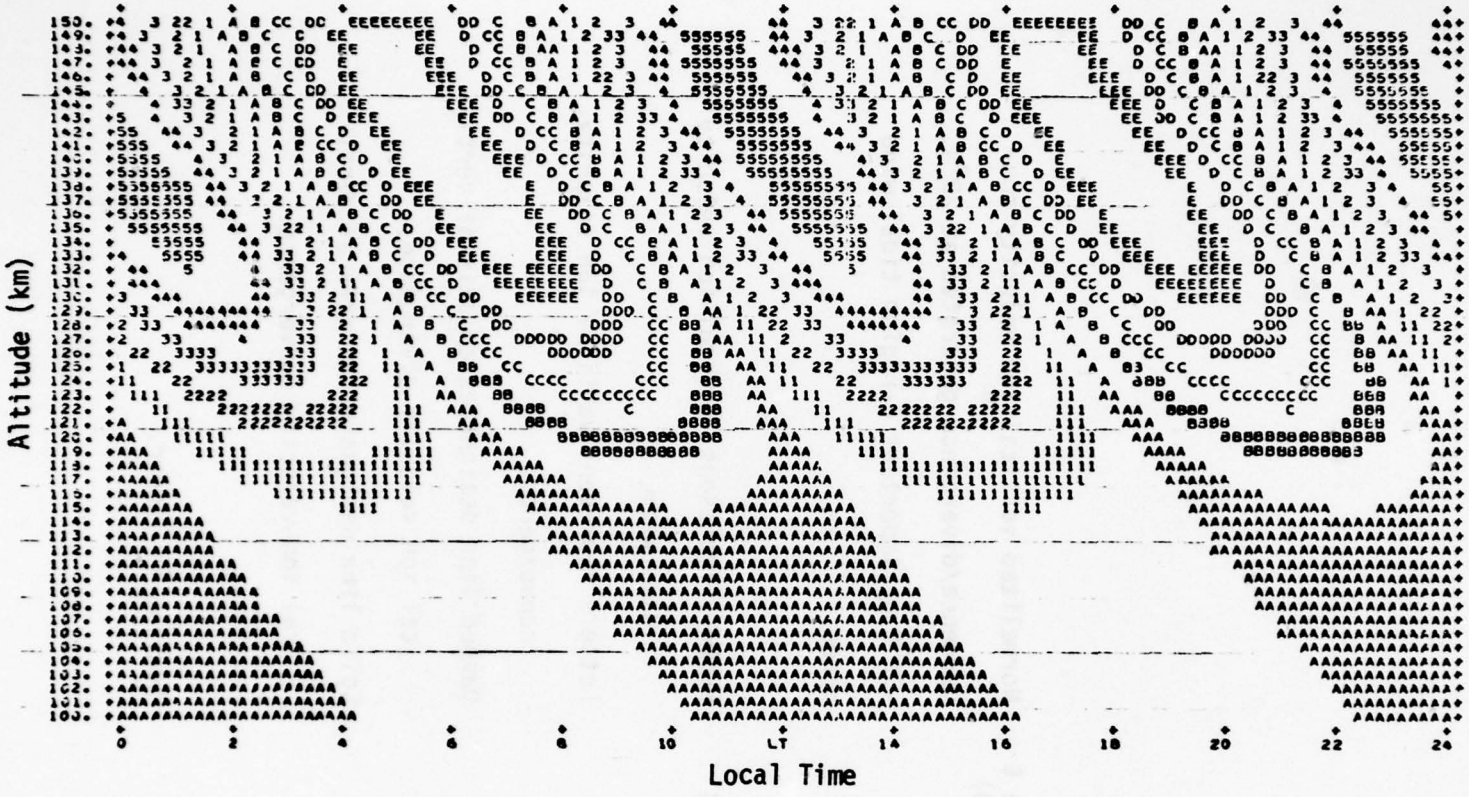



Figure 5(d) (2, 4) mode.

Figure 6 (a-d) Normalized vertical ion velocity convergence/divergence generated at $20^{o}N$, $-70^{o}E$ by important E-region tidal wind modes.

Legend: Numbers represent vertical ion velocity divergence.

Letters represent vertical ion velocity convergence.

Dashed line designates an axis of vertical ion velocity divergence.

Solid line designates an axis of vertical ion velocity convergence.

Note: Scaling is linear.

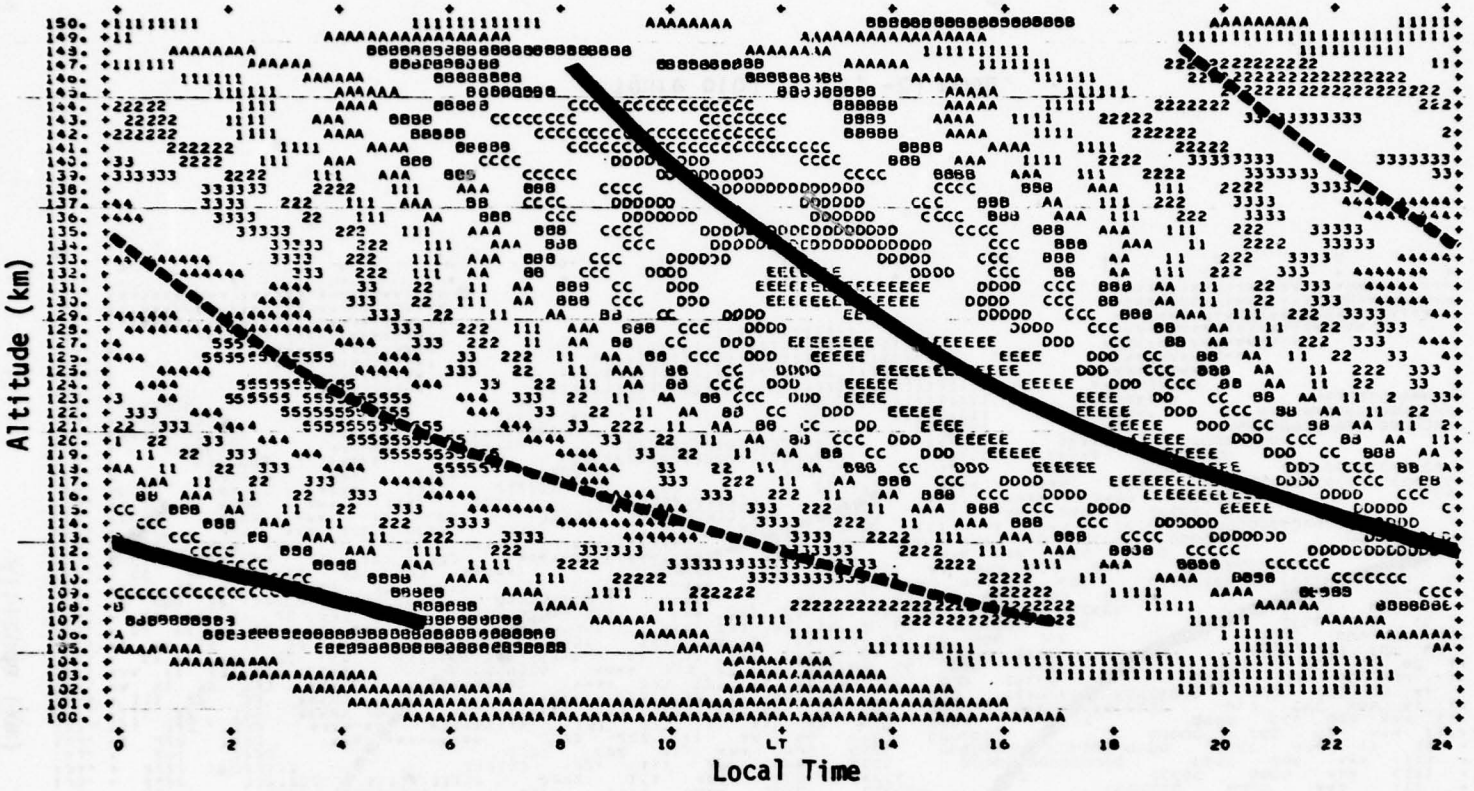



Figure 6(a) (1, 1) mode.

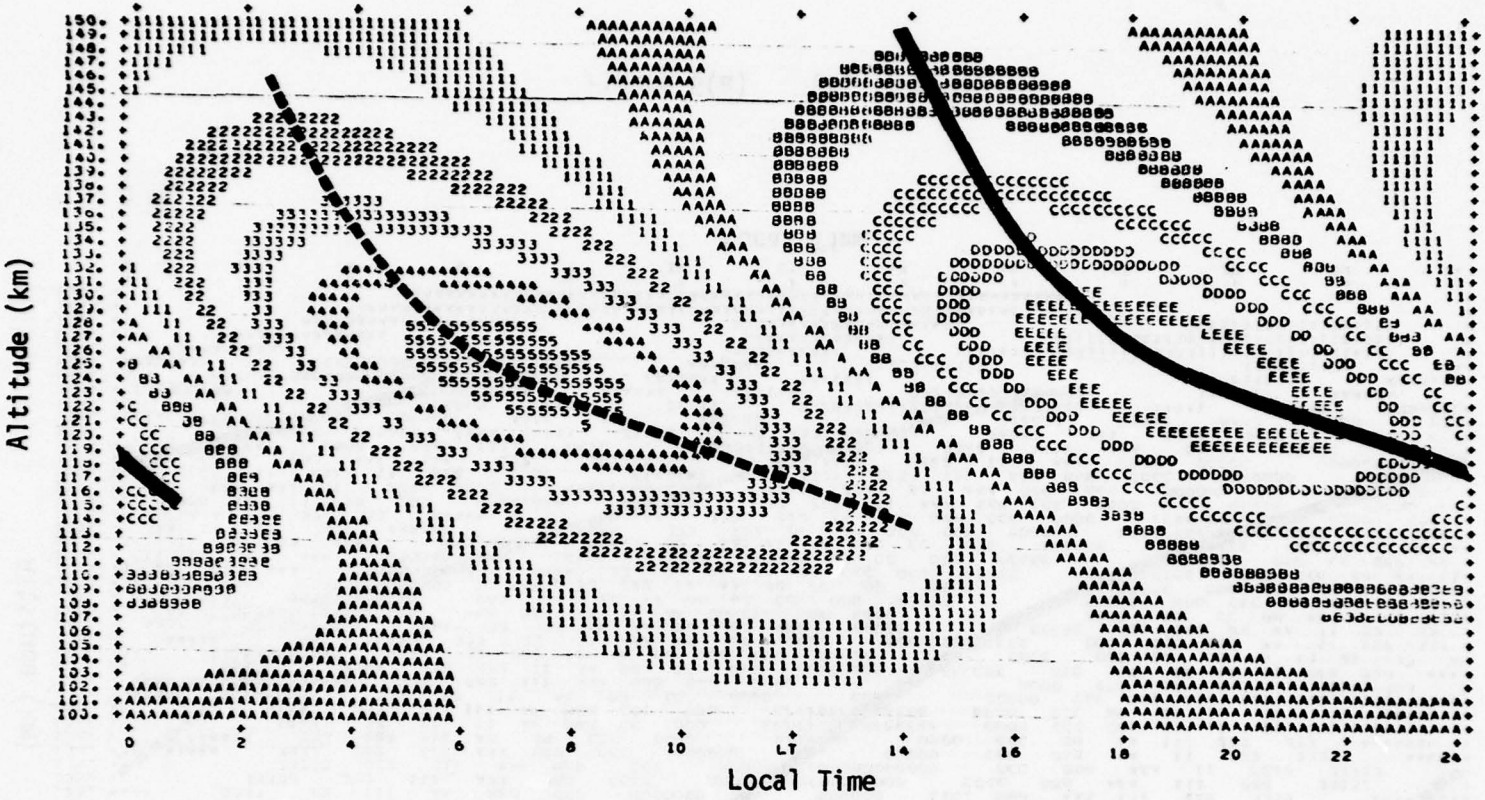



Figure 6(b) (1, -2) mode.

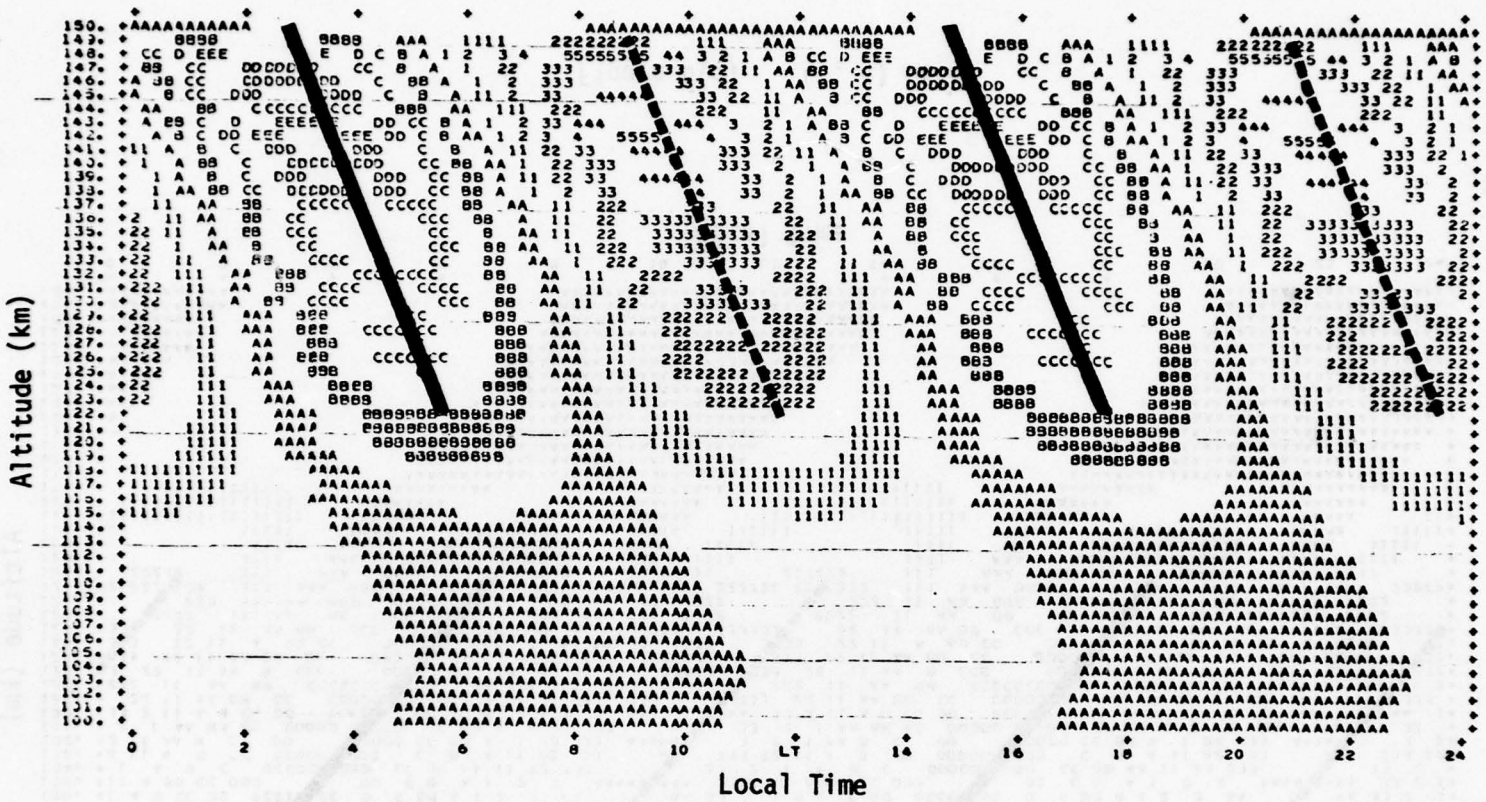



Figure 6(c) (2, 2) mode.

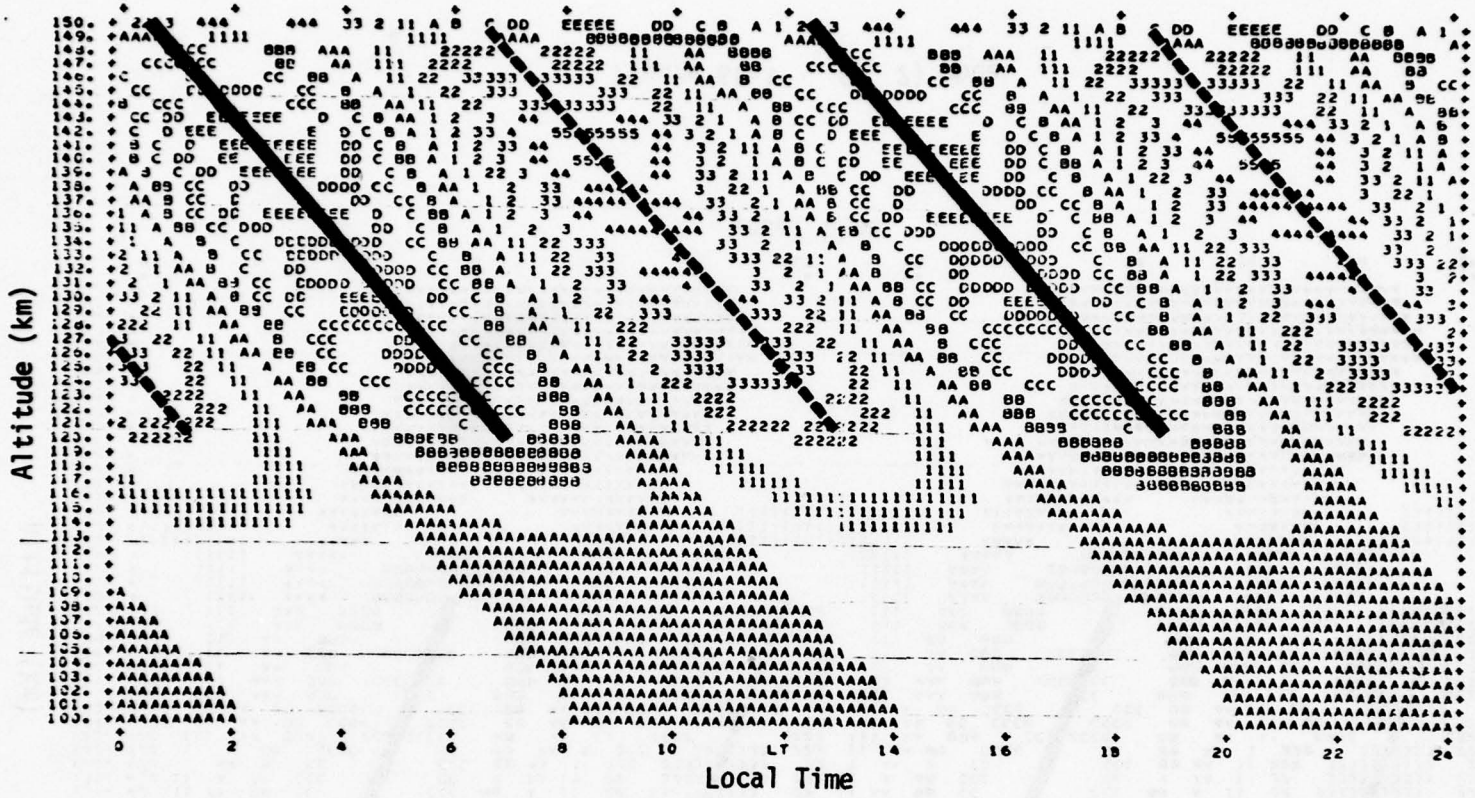



Figure 6(d) (2, 4) mode.

a) Sporadic-E layers produced by the propagating tidal wind modes tend to form in the upper E-region and propagate downwards into the mid and lower E-region over a period of 6 to 12 hours. Therefore, it can be stated that tidally-driven $E_s$ layers generally mimic the behavior of sequentially sporadic-E.

b) The vertical propagation velocity of $E_s$ generated by the evanescent (1, -2) mode is a strong function of latitude (see Table 2). In particular, for latitudes north of $30^o$, the numerical simulations indicate that the (1, -2) mode can actually generate upward-propagating sporadic-E layers.

c) The diurnal modes produce their greatest convergence at altitudes around 125 km. This characteristic is largely independent of latitude.

d) In general, the semidiurnal modes produce their greatest convergence at altitudes near 140 km.

e) For the tidal wind modes under consideration, the wind-shear ion convergence mechanisms numerically dominate the non-shear convergence mechanisms by factors ranging from 1.5 to 3.

f) The overall convergence pattern for the (2, 4) mode shifts 6 hours ($90^o$) as $30^o$ latitude is traversed. This effect is produced by the (2, 4) tidal wind node situated near $30^o$-$35^o$ latitude. (See Figure 4.)

g) The vertical phase propagation velocity is distinctly different for each of the tidally-driven $E_s$ modes. In general,

sporadic-E layers formed by the semidiurnal tidal wind modes propagate vertically downwards at a rate 2 to 4 times faster than $E_s$ layers driven by the propagating (1, 1) diurnal mode.

h) The magnitudes of the vertical ion velocity convergences produced by representative atmospheric tidal wind velocities ($|\underline{U}| \approx$ 10 to 50 m/s) are consistent with ion convergences actually measured in sporadic-E layers ($10^{-2}$ to $10^{-3}$ $sec^{-1}$: MacLeod, 1964).

i) The maximum wind-driven ion convergence occurs near $20^{o}$ latitude for all propagating tidal wind modes which were studied. This is not true for the evanescent (1, -2) mode.

Zonal wind effects:

The effects of a vertically-shearless, east-west horizontal (zonal) wind on the production of sporadic-E also has been numerically evaluated. The results of the calculations for a vertical cross-section along the zero magnetic meridian ($\approx -70^{o}$ E. longitude) are shown in Figure 7. This figure shows that a mean, west-to-east zonal wind is most effective in enhancing the formation of sporadic-E in the upper E-region ($\approx$ 140 km) and at lower latitudes. In the same figure, it can be seen that zonal winds aid in the dissipation of $E_s$ layers below 125 km. The results simply reverse if the effects of a mean east-to-west zonal wind are considered. Peak convergences and divergences for a mean zonal wind speed of 10 m/s are on the order of $.2 \times 10^{-3}$ $sec^{-1}$ at low latitudes. This implies that zonal wind

Figure 7 Normalized vertical ion velocity convergence and divergence produced by a mean, west-to-east, zonal wind.

Legend: Letters represent vertical ion velocity convergence.
Numbers represent vertical ion velocity divergence.

Note: Scaling is linear.

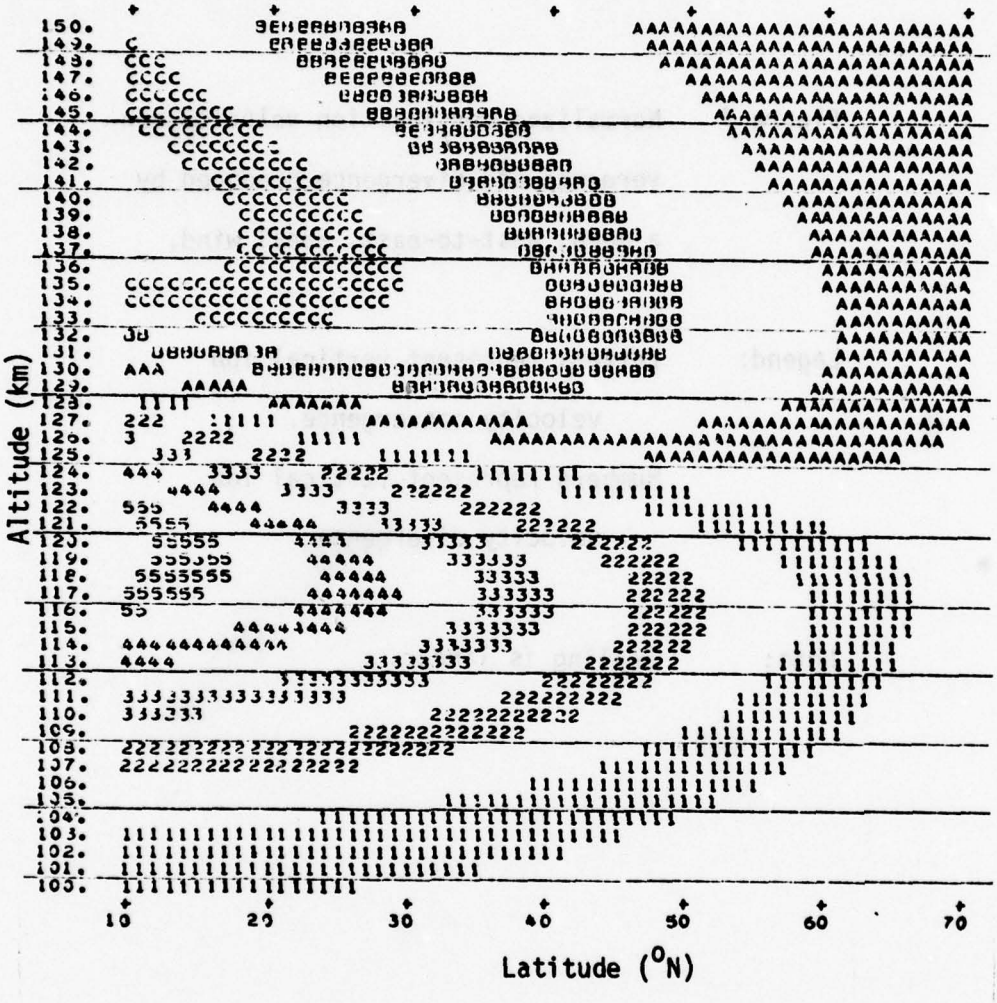
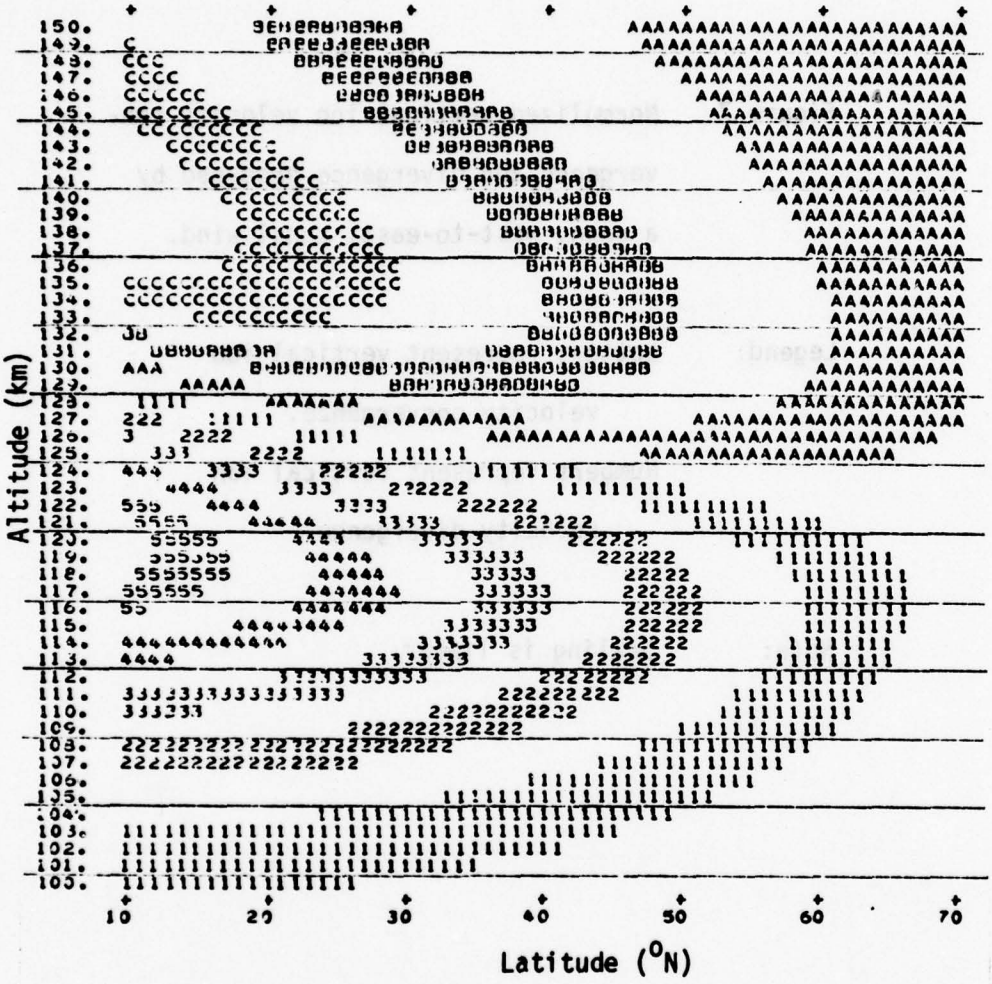

Altitude (km)
150.
149.
148.
147.
146.
145.
144.
143.
142.
141.
140.
139.
138.
137.
136.
135.
134.
133.
132.
131.
130.
129.
128.
127.
126.
125.
124.
123.
122.
121.
120.
119.
118.
117.
116.
115.
114.
113.
112.
111.
110.
109.
108.
107.
106.
105.
104.
103.
102.
101.
100.
10
20
30
40
50
60
70
Latitude (°N)

Figure 7 Normalized vertical ion velocity convergence and divergence produced by a mean, west-to-east, zonal wind.

Legend: Letters represent vertical ion velocity convergence.
Numbers represent vertical ion velocity divergence.

Note: Scaling is linear.


Altitude (km)
Latitude (°N)
10
20
30
40
50
60
70

effects are approximately an order of magntitude smaller than the ion convergences generated by the propagating tidal winds.

## Summary

In this chapter, the details of the construction of a tidally-driven, numerical sporadic-E model were discussed, and results of several simulations were presented. The results indicate that $E_s$ layers theoretically can be produced by vertical ion convergences generated by atmospheric tidal winds. Furthermore, the simulations indicate that each different tidal wind mode produces a sporadic-E layer with a distinct set of behavioral characteristics. Therefore, by studying observed spatial and temporal patterns of sporadic-E, it may be possible to identify and study the important diurnal and semi-diurnal atmospheric tidal wind modes. This particular problem will be considered in the next chapter.

# IV. COMPARISON OF THEORETICAL RESULTS WITH SPORADIC-E DATA

In the previous chapter, the spatial and temporal ion convergence and divergence patterns for selected atmospheric tidal wind modes were presented. In this chapter, the results of these theoretical numerical computations will be compared to published sporadic-E data.

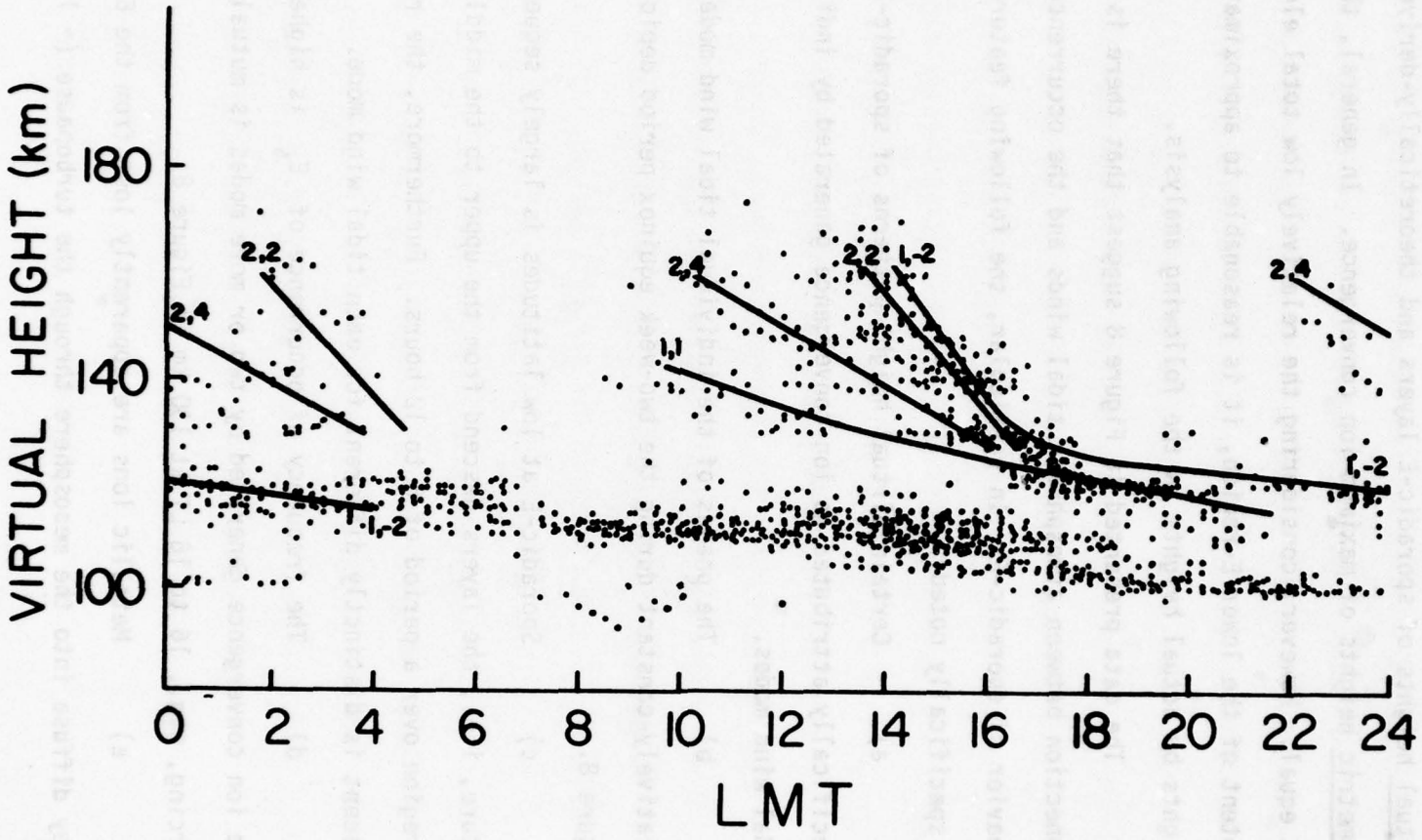
The task of evaluating theoretical $E_s$ model predictions is greatly hampered by the paucity of useful sporadic-E data. In general, most published sporadic-E data are climatological in nature. Hence, detailed evidence which might confirm specific features predicted by a sporadic-E model is usually not available. The evaluation of $E_s$ model results is further limited by current ionosonde data reporting standards. Under the present URSI ionogram reporting system, the virtual height of <u>only one</u> sporadic-E layer can be reported during any given observation period (usually 1 hour). However, as noted in the first chapter, the presence of more than one $E_s$ layer in the ionosphere is common (see Figure 1, profile 1). Since sporadic-E layers in the lower E-region tend to be more concentrated in comparison to $E_s$ layers in the early stages of formation in the upper E-region, the lower layers are reported and the higher layers are ignored. Also, since sporadic-E layers with critical frequencies less than .5 MHz are not reported under the URSI system, the embryonic behavior of high-level sequential sporadic-E is largely undocumented. The usefulness of Central Radio Propagation Laboratory

(CRPL) sporadic-E data is also severely limited by the poor virtual height resolution (5 km) used in the reporting system. This coarse height resolution particularly inhibits the accurate computation of the vertical phase propagation velocity of sequential sporadic-E. Finally, since most ionosonde stations have been established for the primary purpose of observing and reporting the behavior of photochemically-produced E- and F-region ionization, it is not uncommon to find many stations operating on daytime schedules only. Therefore, comprehensive studies of night-time sporadic-E are not easily conducted.

In order to circumvent the limitations of the present world-wide ionosonde data reporting system, MacDougall (1974a,b) has hand-analyzed numerous unreduced ionograms for the expressed purpose of accurately determining the virtual heights of sporadic-E layers as a function of time. The dots in Figure 8 represent occurrences of sporadic-E over Jamaica ($20^{o}$ N, $-70^{o}$E) as determined by MacDougall. The lines in Figure 8 have been transcribed from Figures 6(a) through 6(d). They represent the theoretically-computed axes (or planes) of vertical ion velocity convergence which are formed by using Richmond's (1971) tidal winds as the forcing function in the numerical sporadic-E model presented in the previous chapter.

At this point, it is important to recognize that the analysis presented in Figure 8 represents a comparison between the

Figure 8 Analysis of sporadic-E virtual height data for Jamaica ($20^{o}$N, $-70^{o}$E) for 1-15 March 1965.


VIRTUAL HEIGHT (km)
180
140
100
0
2
4
6
8
10
12
14
16
18
20
22
24
LMT
2,4
2,2
1,-2
1,1
2,4
2,2
1,-2
2,4
1,-2

virtual heights of sporadic-E layers and theoretically-derived, geometric heights of maximum ion convergence. In general, they are not equal. However, considering the relatively low total electron content of the lower E-region, it is reasonable to approximate virtual heights by actual heights in the following analysis.

The data presented in Figure 8 suggest that there is a strong connection between atmospheric tidal winds and the occurrence and behavior of sporadic-E. In particular, the following features should be specifically noted:

a) Certain virtual height patterns of sporadic-E can be specifically attributed to ion convergence generated by individual tidal wind modes.

b) The phases of the individual tidal wind modes remain relatively constant during the two-week equinox period depicted in Figure 8.

c) Sporadic-E at low latitudes is largely sequential in nature, i.e., the layers descend from the upper to the middle and lower E-region over a period of 6 to 12 hours. Furthermore, the rate of descent is distinctly different for each tidal wind mode.

d) The frequency of occurrence of $E_s$ is highest where the ion convergence generated by two or more modes is mutually reinforcing, e.g., 16 to 18 LT at 130 km in Figure 8.

e) Metallic ions are apparently lost from the E-region as they diffuse into the mesosphere through the turbopause (~ 100 km).

The lines in Figure 8 represent only the axes of maximum vertical ion velocity convergence for the selected tidal wind modes. However, corresponding to each axis of ion convergence is an axis of vertical ion velocity divergence (see Figures 6(a) through 6(d)). The lines of maximum ion divergence corresponding to the lines of convergence drawn in Figure 8 are shown separately in Figure 9. The axes of ion divergence shown in Figure 9 explain several interesting features of Figure 8.

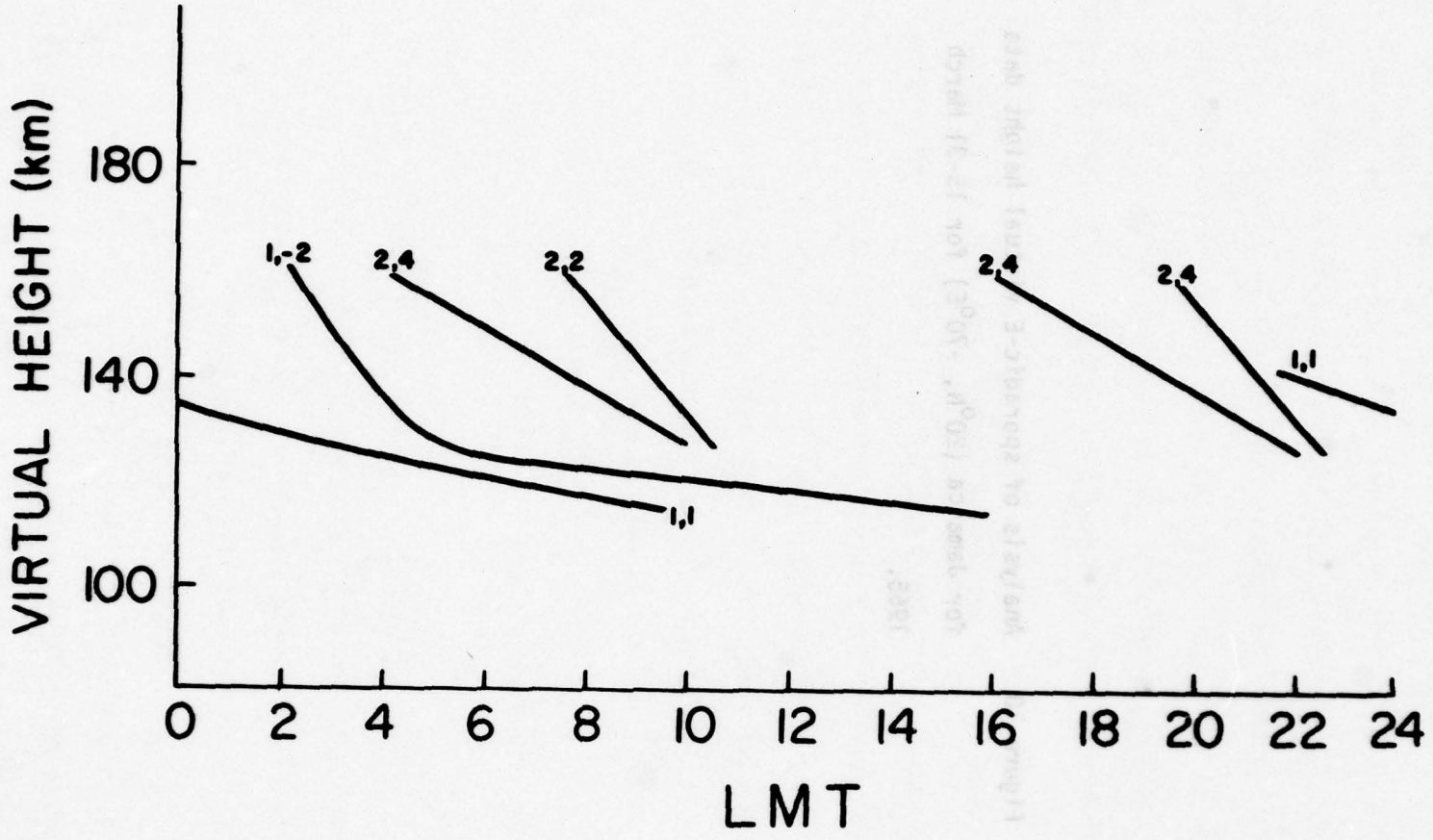
a) The low frequency of occurrence of sporadic-E during early morning hours (0-10 LT) can be partly explained by the mutual reinforcement of the combined divergence patterns of the four tidal wind modes. The fact that much of the neutral metallic debris entering the atmosphere during the night is not photoionized until sunrise is undoubtably an additional contributing factor.

b) The "ion notch" (i.e., depression of $E_s$ virtual height) seen at 120 km between 7 and 12 LT in Figures 8 and 10 can be conveniently explained by the axis of ion divergence for the (1, 1) mode (see Figure 9).

Figure 10 shows the occurrences of sporadic-E observed during the second half of March, 1965 at Jamaica By carefully comparing the data in Figures 8 and 10, several noteworthy observations regarding the temporal behavior of sporadic-E can be made:

a) The phases of all of the vertically-propagating modes ((1, 1), (2, 2), (2, 4)) has shifted approximately 1 hour during the one month period of observation. This suggests that the phases of the tidal winds may be functions of the time of year.

Figure 9 Axes (or planes) of ion divergence corresponding to the axes of ion convergence depicted in Figure 8.


VIRTUAL HEIGHT (km)
180
140
100
1,-2
2,4
2,2
1,1
2,4
2,4
1,1
0
2
4
6
8
10
12
14
16
18
20
22
24
LMT

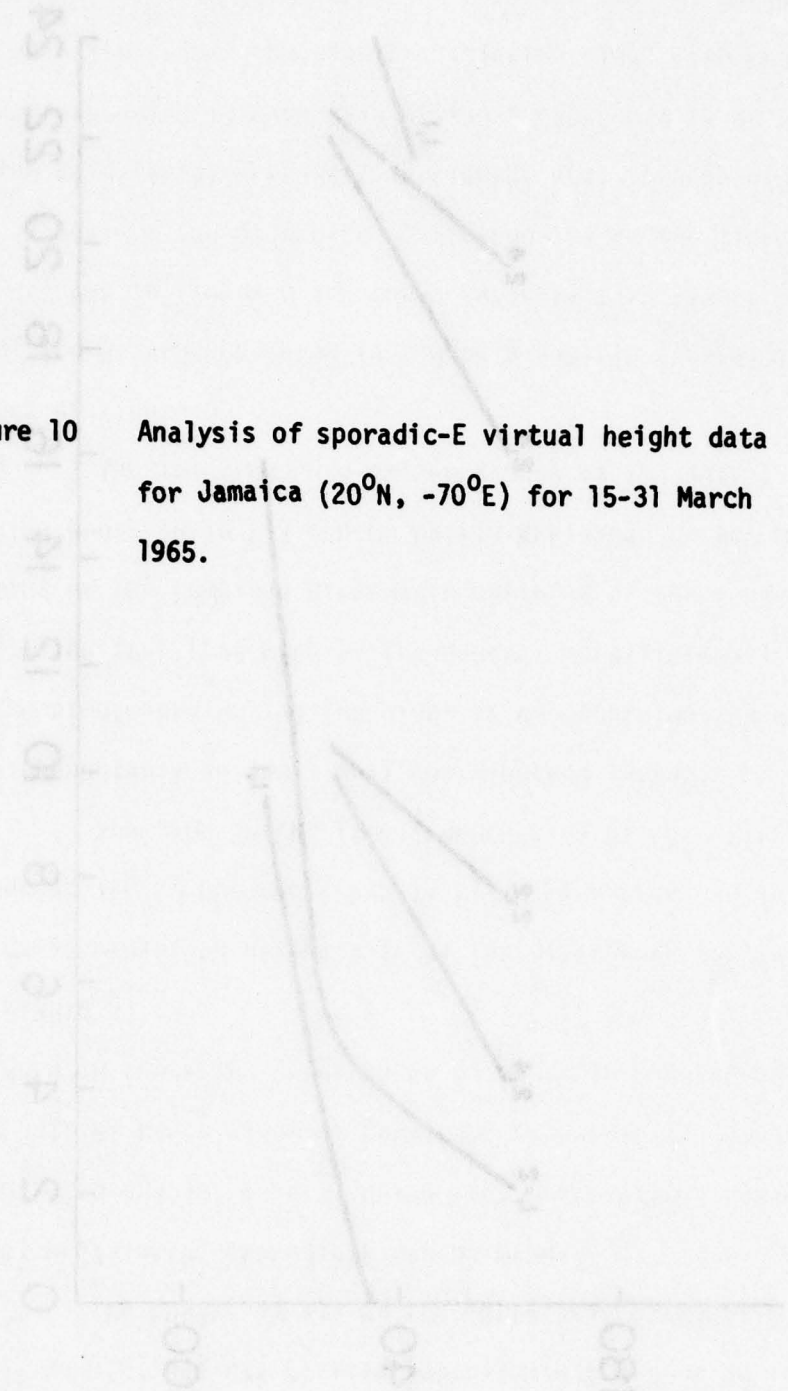
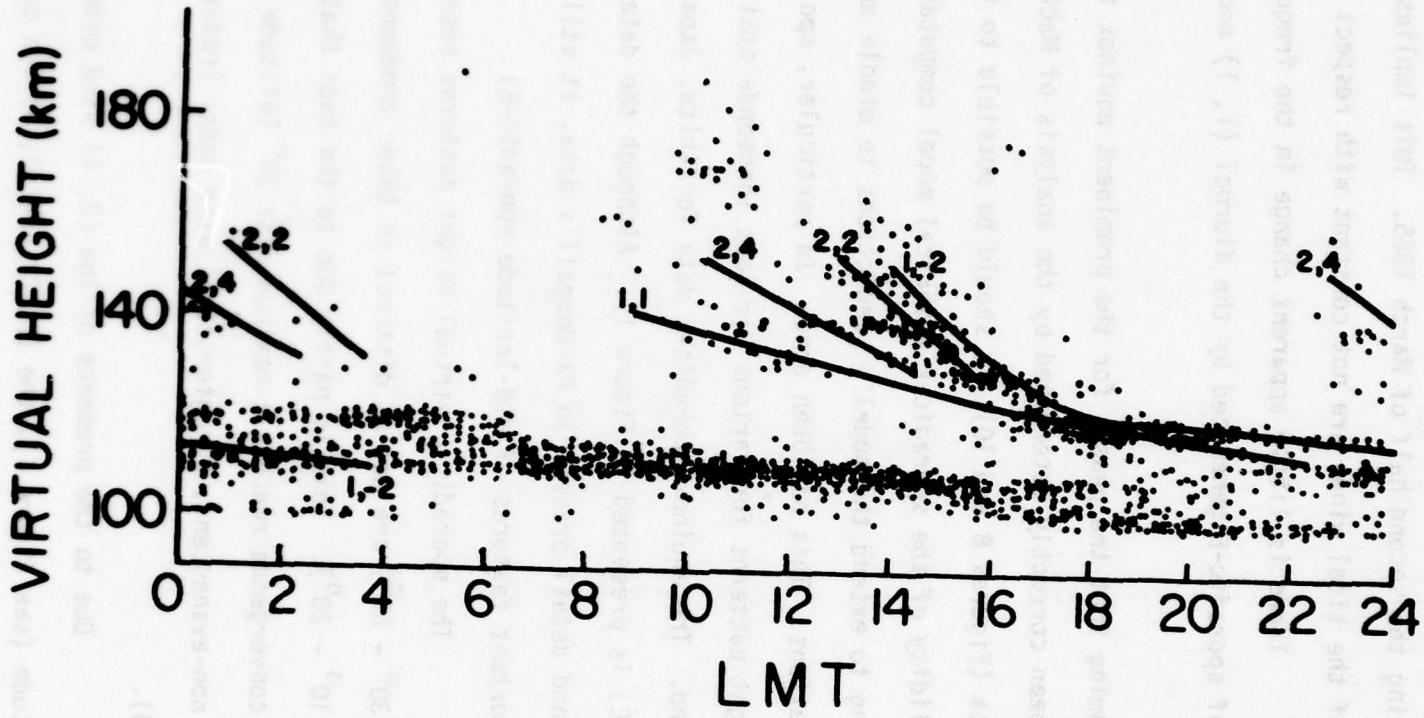


Figure 10 Analysis of sporadic-E virtual height data for Jamaica ($20^{O}$N, $-70^{O}$E) for 15-31 March 1965.


VIRTUAL HEIGHT (km)
180
140
100
0
2
4
6
8
10
12
14
16
18
20
22
24
LMT
2,2
2,4
1,-2
1,1
2,4
2,2
1,-2
2,4
1,-2

b) Production of sporadic-E by the (2, 4) tidal wind mode declined during the second half of March 1965. This implies that the amplitudes of the tidal winds are not constant with respect to time.

c) There is little apparent change in the frequency of occurrence of sporadic-E generated by the diurnal (1, 1) and (1, -2) winds.

Assuming that the phases for the prominent equinox tidal wind modes have been correctly determined by the analysis of MacDougall's Jamacian data (Figures 8 and 10), it should be possible to further test the validity of the sporadic-E numerical model computations by attempting to extend the model's predictions to middle and high latitude stations. This has been done. In particular, sporadic-E virtual height patterns for various Far East ionosonde stations have been analyzed. The equinox sporadic-E data for Akita, Japan ($39^{o}$N, $140^{o}$E) is presented in Figure 11. Although the data lacks the resolution and detail present in MacDougall's data, it still illustrates several important features of mid-latitude sporadic-E:

a) The sporadic-E virtual height patterns seen at mid-latitudes ($30^{o}$ - $60^{o}$) are not as distinct as those produced at low latitudes ($10^{o}$ - $20^{o}$). This is partly due to the fact that tidally-driven ion convergence reaches a maximum near $20^{o}$ latitude for the important, non-evanescent, E-region tidal wind modes (reference Tables 1 through 4).

b) Due to the presence of the (2, 4) wind nodes near $\approx 30^{o}$ latitude (see Figure 4), the (2, 2) and (2, 4) ion convergence and divergence patterns are out of phase with respect to each other

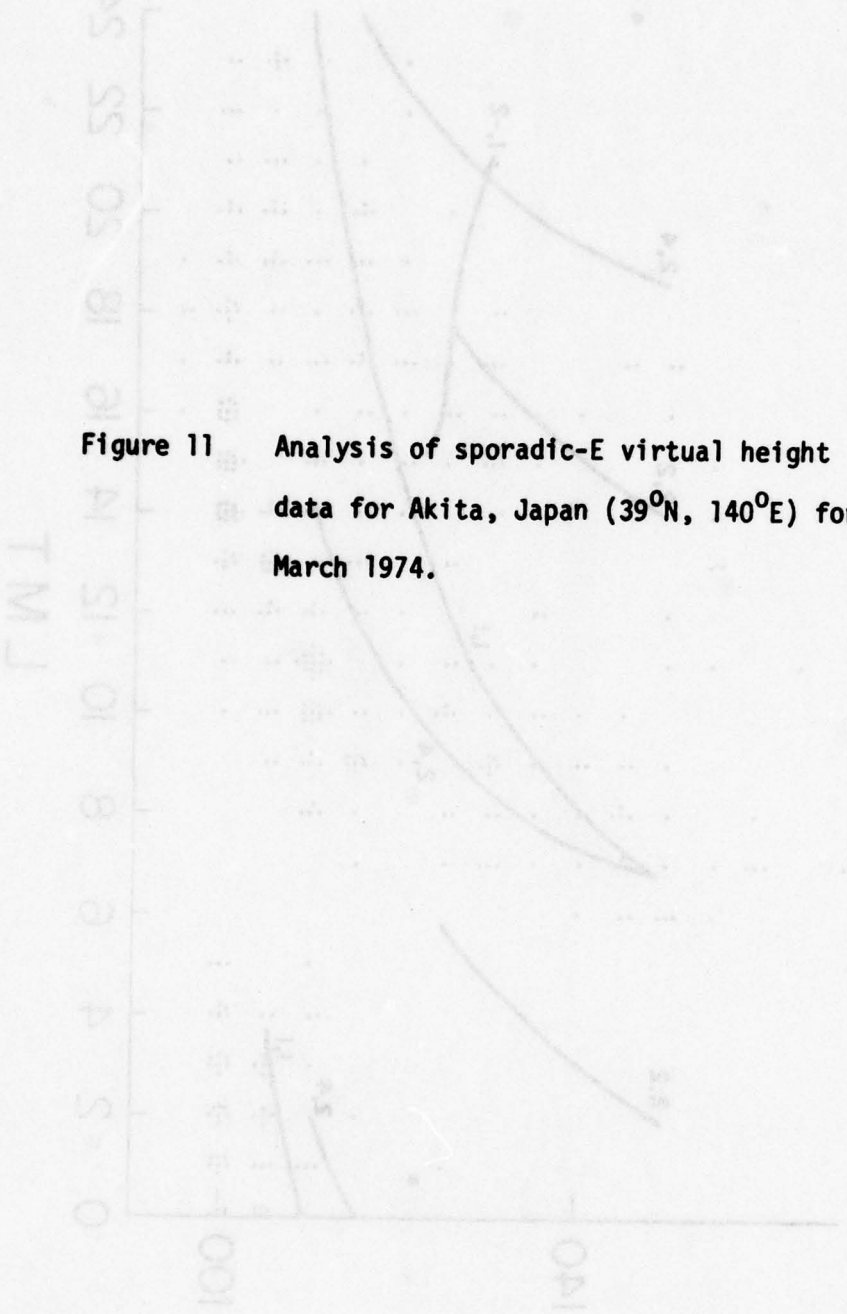
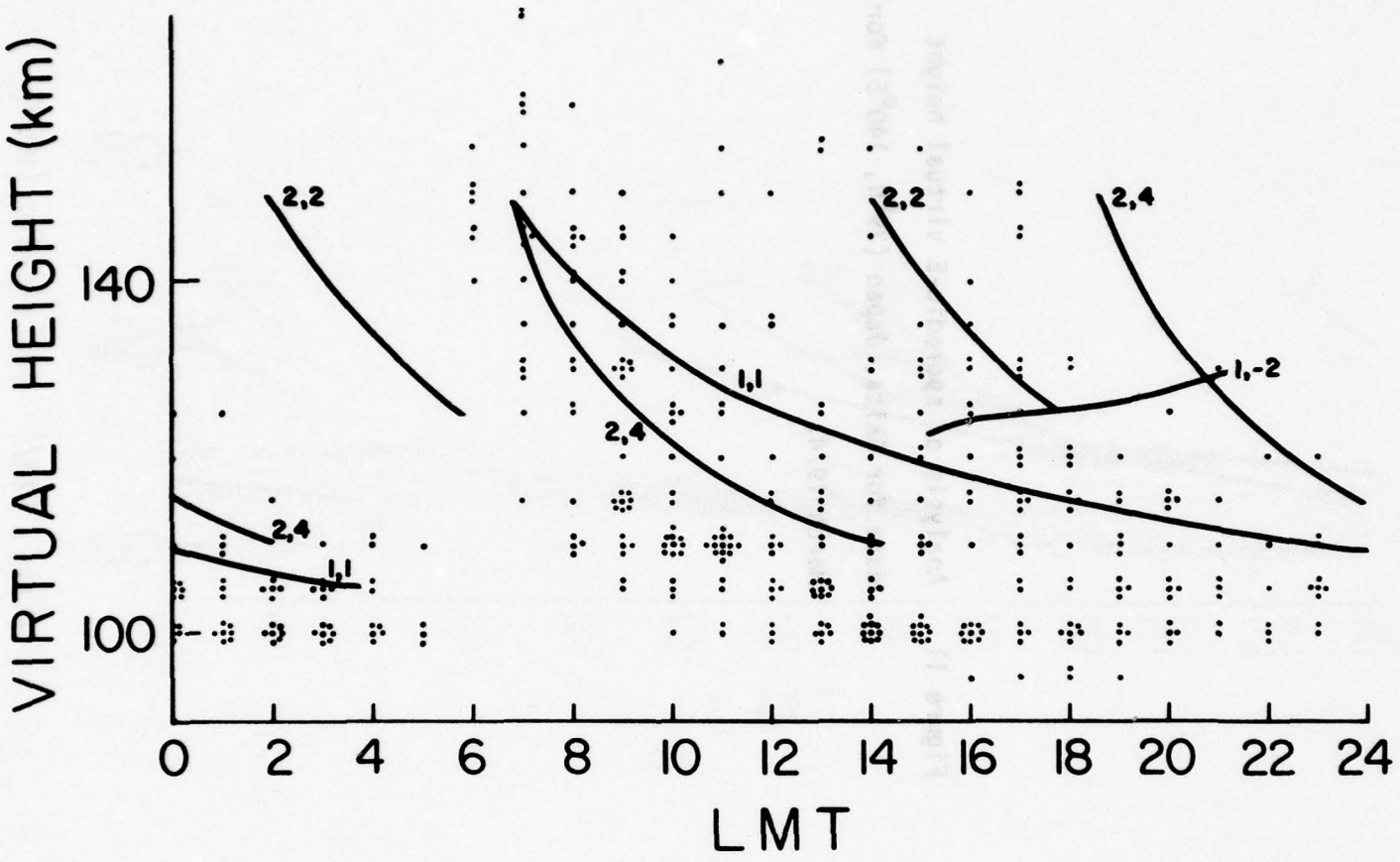


Figure 11 Analysis of sporadic-E virtual height data for Akita, Japan (39°N, 140°E) for March 1974.


VIRTUAL HEIGHT (km)
140
100
0
2
4
6
8
10
12
14
16
18
20
22
24
LMT
2,2
2,4
1,1
2,2
2,4
1,1
1,-2

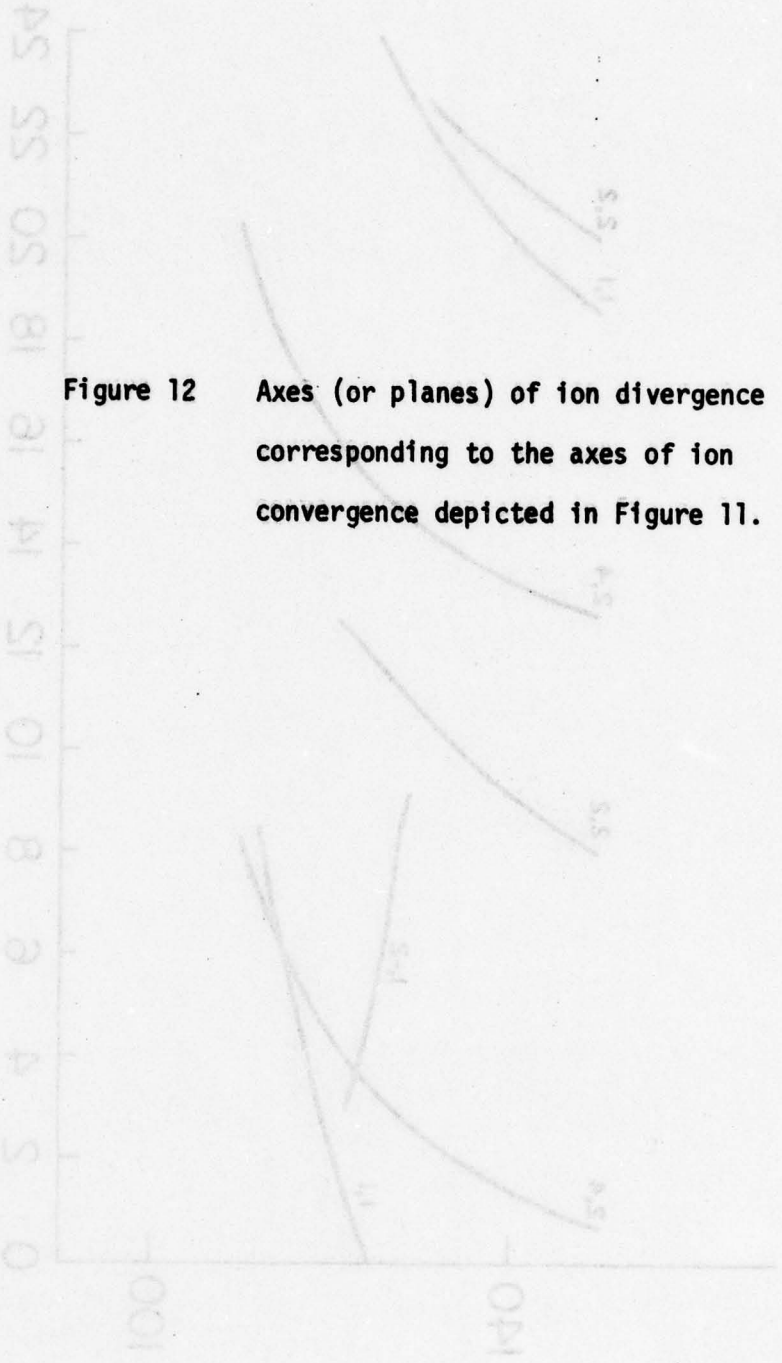
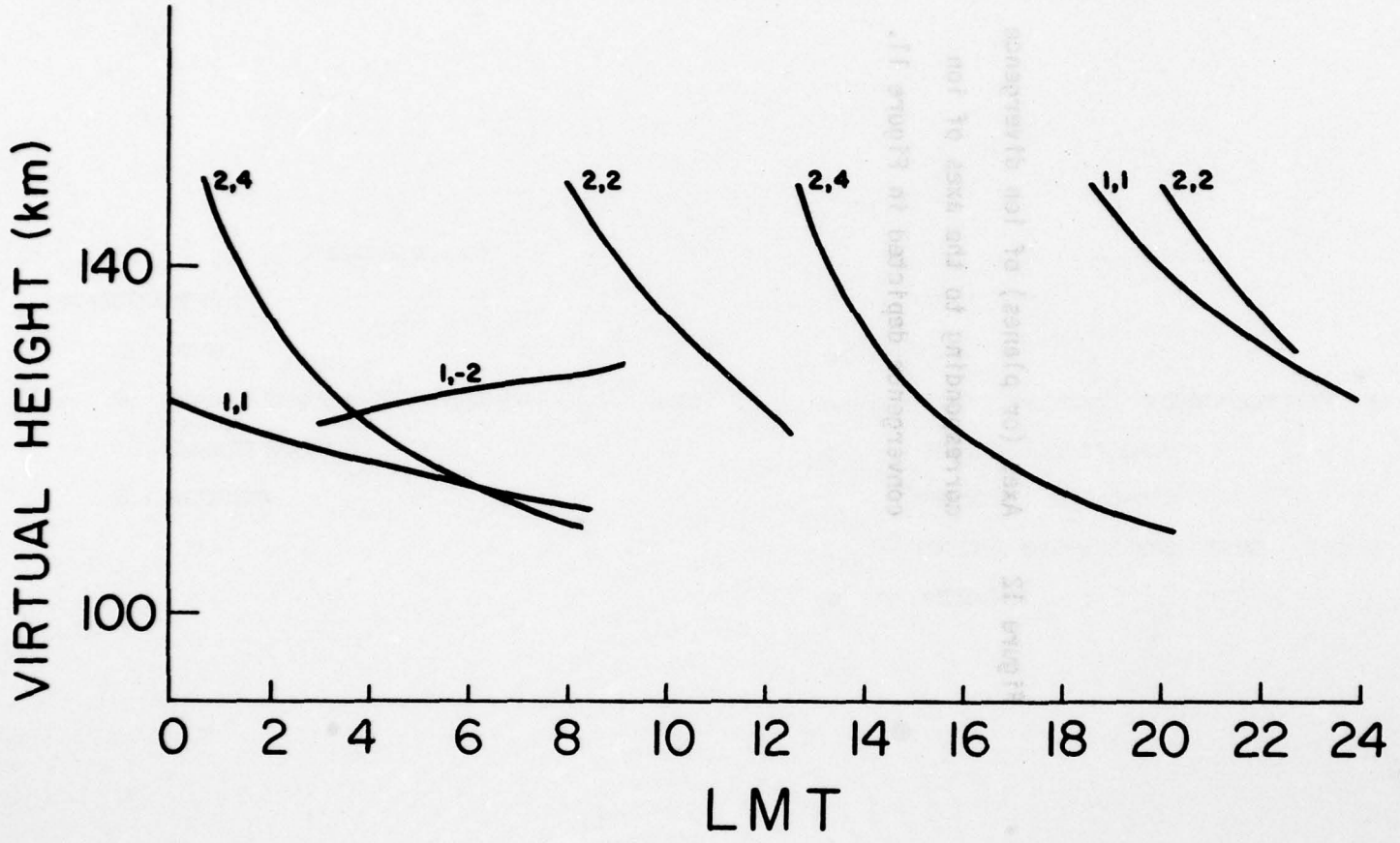


Figure 12 Axes (or planes) of ion divergence corresponding to the axes of ion convergence depicted in Figure 11.


VIRTUAL HEIGHT (km)
140
100
2,4
2,2
2,4
1,1
2,2
1,-2
1,1
0
2
4
6
8
10
12
14
16
18
20
22
24
LMT

at latitudes greater than $30^{o}$. Consequently, they destructively interfere with one another (see Figures 11 and 12). Therefore, the mid-latitude ion convergence patterns produced by the semidiurnal tides are not as distinct as the patterns depicted in low-latitude $E_s$ data, e.g., Figures 8 and 10. (*See footnote at end of chapter.)

c) The (1,-2) mode produces <u>ascending</u> $E_s$ layers at mid-latitudes. This behavior is contrary to the descending ion convergence patterns produced by the other tidal wind modes. As such, the (1, -2) ion convergence pattern adds considerable complexity to depictions of sporadic-E occurrences at middle and high latitudes.

d) The ion convergence patterns produced by the (1, 1) and (2, 4) modes at mid-latitudes are nearly in phase during the morning hours (6-12 LT). Accordingly, the strong convergence generated by the mutual interaction of these modes is clearly evident in the sporadic-E virtual height patterns for Akita (Figure 11).

As an aside, it should again be reemphasized that the phases of the tidal winds used in the comparison of the theoretical and observational results presented in this chapter were empirically chosen to maximize the agreement between MacDougall's data and the $E_s$ numerical model predictions. Nonetheless, the semidiurnal tidal wind phases used for the analysis of the sporadic-E patterns in Figures 8 and 10 are in good agreement with wind phases independently deduced from the analysis of magnetic field variations produced by tidally-driven ionospheric currents. (Unpublished work at UCLA.)

Specifically the (2, 4) phases are virtually equal while the (2, 2) phases differ by 1.5 hours ($\approx 22^{o}$). The determination of the phase of the (1, -2) tide from sporadic-E data is somewhat more uncertain. Although the axis of maximum ion convergence for the (1, -2) mode appears to be properly placed in the Jamacian data, it seems that a better agreement with the Akita, Japan data can be made if the phase is shifted minus 4 hours. The overall difficulty in accurately determining the phase of the (1, -2) tidal wind is in part due to the fact that the (1, -2) mode is not particularly effective in producing ion convergence in the E-region (see Table 2). Hopefully, this problem can be overcome through the analysis of more mid-latitude ionosonde data since the (1, -2) mode produces its maximum ion convergence near $40^{o}$ latitude.

Summary:

The purpose of this chapter was to clearly demonstrate the fact that atmospheric tidal winds play a distinct and important role in the formation and vertical propagation of sequential sporadic-E. In particular, it was shown that Richmond's (1971) tidal wind formulation, when used as the forcing function in a numerical sporadic-E model, correctly predicts the broad features of equinox $E_s$ for two widely-separated stations situated at different latitudes.

*The statistical significance of the Akita, Japan $E_s$ data is presently being improved by including Vernal equinox data for several years.

# V. CONCLUSIONS

The most interesting aspects of the mathematical analysis and observational evidence presented in the previous chapters can be briefly summarized as follows:

a) The gross features of the convergence of metallic ions in the ionospheric E-region (sporadic-E) can be adequately explained by considering a steady-state equilibrium between neutral wind motions and the resultant collisional and geomagnetic forces experienced by the ions in the neutral gas.

b) Representative tidal wind velocities generate sufficient ion convergence to account for the observed formation of sporadic-E layers.

c) Each tidal wind mode generates a theoretically-distinct pattern of vertical ion velocity convergence. Each characteristic pattern is a function of geographic and geomagnetic latitude.

d) Occurrences of sporadic-E attributable to ion convergence generated by individual tidal wind modes have been identified in composite, low-latitude $E_s$ data. As such, it has been possible to estimate the phases of the important E-region tidal wind modes.

e) Having estimated the phases and approximate amplitudes of the tidal winds at a given location, it is theoretically possible to describe the gross temporal patterns of sporadic-E which should be observed at other latitudes and longitudes. This hypothesis has been put to a test through the analysis of equinox sporadic-E data from Jamaica and Japan.

At present, the predictive capabilities of the numerical sporadic-E model which has been presented seem promising. However, the ultimate usefulness of the model will have to be determined through the careful analysis of more, global sporadic-E data.

## APPENDIX 1

Derivation of the ion velocity resulting from mechical and electrostatic forcing of a collisional, magnetic, weakly-ionized plasma (e.g., the ionospheric plasma).

In general, the equation of motion for ions in the earth's ionospheric E-region can be written as

$$m_i n_i \frac{d\underline{V}_i}{dt} = m_i n_i \nu_{in} (\underline{U} - \underline{V}_i) + q_i n_i \left( \underline{E} + \frac{\underline{V}_i \times \underline{B}}{C} \right) + m_i n_i \underline{g} - \nabla P_i \qquad (1.1)$$

where: $m_i$ ≡ ion mass

$n_i$ ≡ ion concentration

$\underline{V}_i$ ≡ ion velocity

$\nu_{in}$ ≡ ion neutral collision frequency

$\underline{U}$ ≡ neutral wind velocity

$q_i$ ≡ ion charge

$\underline{E}$ ≡ electrostatic field vector

$\underline{B}$ ≡ magnetic field vector

$C$ ≡ speed of light

$\underline{g}$ ≡ gravitational vector

$\nabla P_i$ ≡ ion partial pressure gradient

For externally-forced ion motions in the ionospheric E-region, the Lorentz and collisional forces dominate the gratitational and

ion partial pressure gradient forces. (See main text for a detailed discussion.) Therefore, by neglecting the ion partial pressure gradient and gravitational terms, the steady-state equation of motion simplifies to:

$$m_i n_i \nu_{in} (\underline{U} - \underline{V}_i) + q_i n_i \left( \underline{E} + \frac{\underline{V}_i \times \underline{B}}{C} \right) = 0$$

which can be rewritten as:

$$\nu_{in} (\underline{U} - \underline{V}_i) + \frac{q_i |\underline{B}|}{m_i C} \left( \frac{C\underline{E}}{|\underline{B}|} + \frac{\underline{V}_i \times \underline{B}}{|\underline{B}|} \right) = 0 \qquad (1.2)$$

By defining the following quantities:

$$\omega_i \equiv \frac{e|\underline{B}|}{m_i C} \quad : \quad \text{ion gyro frequency}$$

$$\underline{\varepsilon} \equiv \frac{C\underline{E}}{|\underline{B}|} \quad : \quad \text{reduced electric field}$$

$$\hat{b} \equiv \frac{\underline{B}}{|\underline{B}|} \quad : \quad \text{unit vector parallel to magnetic field vector}$$

Equation (1.2) becomes:

$$\frac{\nu_{in}}{\omega_i} (\underline{U} - \underline{V}_i) + \underline{\varepsilon} + (\underline{V}_i \times \hat{b}) = 0 \qquad (1.3)$$

Define: $\beta_i \equiv \frac{\nu_{in}}{\omega_i}$ .

Using this, Equation (1.3) can be rewritten:

$$\beta_i \, (\underline{U} - \underline{V}_i) + \underline{\varepsilon} + (\underline{V}_i \times \hat{b}) = 0 \quad . \tag{1.4}$$

Crossing Equation (1.4) with $\hat{b}$ , we have:

$$\beta_i \, (\underline{U} \times \hat{b}) - \beta_i \, (\underline{V}_i \times \hat{b}) + \underline{\varepsilon} \times \hat{b} + (\underline{V}_i \times \hat{b}) \times \hat{b} = 0 \tag{1.5}$$

Next, recall that:

$$(\underline{V}_i \times \hat{b}) \times \hat{b} = - \underline{V}_i \, (\hat{b} \cdot \hat{b}) + (\underline{V}_i \cdot \hat{b}) \, \hat{b}$$

or, since $\hat{b} \cdot \hat{b} = 1$ :

$$(\underline{V}_i \times \hat{b}) \times \hat{b} = - \underline{V}_i + (\underline{V}_i \cdot \hat{b}) \, \hat{b} \tag{1.6}$$

Substituting Equation (1.6) into Equation (1.5):

$$\beta_i \, (\underline{U} \times \hat{b}) - \beta_i \, (\underline{V}_i \times \hat{b}) + \varepsilon \times \hat{b} = \underline{V}_i - (\underline{V}_i \cdot \hat{b}) \, \hat{b} \tag{1.7}$$

From Equation (1.4), we note that:

$$\underline{V}_i = \frac{1}{\beta_i} (\underline{\varepsilon} + (\underline{V}_i \times \hat{b})) + \underline{U} \tag{1.8}$$

and

$$- \beta_i (\underline{V}_i \times \hat{b}) = \beta_i^2 (\underline{U} - \underline{V}_i) + \beta_i \underline{\varepsilon} \tag{1.9}$$

Substituting Equations (1.8) and (1.9) into (1.7):

$$\beta_i (\underline{U} \times \hat{b}) + (\beta_i^2 (\underline{U} - \underline{V}_i) + \beta_i \underline{\varepsilon}) + \underline{\varepsilon} \times \hat{b} =$$

$$\underline{V}_i - \frac{1}{\beta_i} (\varepsilon \cdot \hat{b}) \hat{b} - \frac{1}{\beta_i} (\underline{V}_i \times \hat{b}) \cdot \hat{b} - (\underline{U} \cdot \hat{b}) \hat{b} \tag{1.10}$$

(the term $(\underline{V}_i \times \hat{b}) \cdot \hat{b}$ is crossed out and equals 0)

Equation (1.10) now can can be simply solved for $\underline{V}_i$, the vertical ion velocity for a wind-driven, collisional, magnetic plasma:

$$\underline{V}_i = \left[\frac{1}{1 + \beta_i^2}\right] \left[\beta_i^2 \underline{U} + \beta_i (\underline{U} \times \hat{b}) + (\underline{U} \cdot \hat{b}) \hat{b}\right]$$

$$+ \left[\frac{1}{1 + \beta_i^2}\right] \left[\beta_i \underline{\varepsilon} + \underline{\varepsilon} \times \hat{b} + \frac{1}{\beta_i} (\underline{\varepsilon} \cdot \hat{b}) \hat{b}\right] \tag{1.11}$$

Note that the r.h.s. of Equation (1.11) has six terms. The first three represent the vertical ion velocity contribution from neutral wind forcing. The second three terms represent the contribution from electric fields.

## APPENDIX 2

**Derivation of the ion velocity divergence/convergence resulting from mechanical forcing of the earth's ionospheric plasma.**

The ion velocity, $\underline{V}_i$ , attributable to the collisional coupling between neutral wind motions and ions in a magnetic, weakly-ionized plasma can be readily identified as the first three terms in Equation (1.11), Appendix 1:

$$\underline{V}_i = \left[\frac{\beta_i^2}{1+\beta_i^2}\right]\underline{U} + \left[\frac{\beta_i}{1+\beta_i^2}\right](\underline{U} \times \hat{b}) + \left[\frac{1}{1+\beta_i^2}\right](\underline{U}\cdot\hat{b})\ \hat{b} \qquad (2.1)$$

Taking the divergence of Equation (2.1):

$$\nabla\cdot\underline{V}_i = \nabla\left[\frac{\beta_i^2}{1+\beta_i^2}\right]\cdot\underline{U} + \left[\frac{\beta_i^2}{1+\beta_i^2}\right](\nabla\cdot\underline{U}) + \nabla\left[\frac{\beta_i}{1+\beta_i^2}\right]\cdot(\underline{U}\times\hat{b})$$

$$+ \left[\frac{\beta_i}{1+\beta_i^2}\right]\nabla\cdot(\underline{U}\times\hat{b}) + \nabla\left[\frac{1}{1+\beta_i^2}(\underline{U}\cdot\hat{b})\right]\cdot\hat{b} + \left[\frac{1}{1+\beta_i^2}(\underline{U}\cdot b)\right]\nabla\cdot\hat{b} \to 0$$

Expanding terms using vector identities:

$$\nabla \cdot \underline{V}_i = \nabla \left[\frac{\beta_i^2}{1+\beta_i^2}\right] \cdot \underline{U} + \left[\frac{\beta_i^2}{1+\beta_i^2}\right] (\nabla \cdot \underline{U}) \left[\frac{\beta_i}{1+\beta_i^2}\right] \cdot (\underline{U} \times \hat{b})$$

$$+ \left[\frac{\beta_i}{1+\beta_i^2}\right] \left[\hat{b} \cdot (\nabla \times \underline{U}) - \underline{U} \cdot (\nabla \times \hat{b})\right] \rightarrow 0$$

$$+ \left[\left[\frac{1}{1+\beta_i^2}\right] \nabla (\underline{U} \cdot \hat{b}) + (\underline{U} \cdot \hat{b}) \nabla \left[\frac{1}{1+\beta_i^2}\right]\right] \cdot \hat{b} \qquad (2.2)$$

Expanding the last term in Equation (2.2)

$$\left[\left[\frac{1}{1+\beta_i^2}\right] \nabla (\underline{U} \cdot \hat{b}) + (\underline{U} \cdot \hat{b}) \nabla \left[\frac{1}{1+\beta_i^2}\right]\right] \cdot \hat{b}$$

$$= \left[\frac{1}{1+\beta_i^2}\right] \left[\hat{b} \cdot (\hat{b} \cdot \nabla)\, \underline{U} + \underline{U} \cdot \nabla (\hat{b} \cdot \hat{b}) + (\hat{b} \times (\nabla \times \underline{U})) \cdot \hat{b}\right]$$

$\underline{U} \cdot \nabla (\hat{b} \cdot \hat{b}) \rightarrow 0$ ; $(\hat{b} \times (\nabla \times \underline{U})) \cdot \hat{b} \rightarrow 0$

$$+ (\underline{U} \times (\nabla \times \hat{b})) \cdot \hat{b} + (U \cdot \hat{b}) \nabla \left[\frac{1}{1+\beta_i^2}\right] \cdot \hat{b} \qquad (2.3)$$

$(\underline{U} \times (\nabla \times \hat{b})) \cdot \hat{b} \rightarrow 0$

Substituting Equation (2.3) into Equation (2.2), we have the expression for the ion velocity divergence/convergence arising from ion motions collisionally induced by neutral wind motions:

$$\nabla \cdot \underline{V}_i = \nabla \left[ \frac{\beta_i^2}{1 + \beta_i^2} \right] \cdot \underline{U} + \left[ \frac{\beta_i^2}{1 + \beta_i^2} \right] \nabla \cdot \underline{U} + \nabla \left[ \frac{\beta_i}{1 + \beta_i^2} \right] \cdot (\underline{U} \times \hat{b})$$

$$+ \left[ \frac{\beta_i}{1 + \beta_i^2} \right] \hat{b} \cdot (\nabla \times \underline{U}) + \left[ \frac{1}{1 + \beta_i^2} \right] \hat{b} \cdot [(\hat{b} \cdot \nabla) \underline{U}]$$

$$+ (\underline{U} \cdot \hat{b}) \nabla \left[ \frac{1}{1 + \beta_i^2} \right] \cdot \hat{b}$$

## APPENDIX 3

Derivation of the ion velocity divergence/convergence resulting from the electrostatic forcing of the earth's ionospheric plasma.

The ion velocity, $\underline{V}_i$ , attributable to motion induced by an electrostatic field in a collisional, magnetic, weakly-ionized plasma can be readily identified as the last three terms in Equation (1.1), Appendix 1.

$$\underline{V}_i = \left[\frac{\beta_i}{1+\beta_i^2}\right] \underline{\varepsilon} + \left[\frac{1}{1+\beta_i^2}\right] (\underline{\varepsilon} \times \hat{b}) + \left[\frac{1}{\beta_i}\right]\left[\frac{1}{1+\beta_i^2}\right] (\underline{\varepsilon}\cdot\hat{b})\,\hat{b} \tag{3.1}$$

Taking the divergence of Equation (3.1)

$$\nabla\cdot\underline{V}_i = \nabla\left[\frac{\beta_i}{1+\beta_i^2}\right]\underline{\varepsilon} + \left[\frac{\beta_i}{1+\beta_i^2}\right](\nabla\cdot\underline{\varepsilon})$$

$$+ \nabla\left[\frac{1}{1+\beta_i^2}\right]\cdot(\underline{\varepsilon}\times\hat{b}) + \left[\frac{1}{1+\beta_i^2}\right]\nabla\cdot(\underline{\varepsilon}\times\hat{b})$$

$$+ \nabla\left[\frac{1}{\beta_i(1+\beta_i^2)}\right]\cdot(\underline{\varepsilon}\cdot\hat{b})\hat{b} + \left[\frac{1}{\beta_i(1+\beta_i^2)}\right]\nabla\cdot((\underline{\varepsilon}\cdot\hat{b})\hat{b})$$

Expanding terms using vector identities:

$$\nabla\cdot\underline{V}_i = \nabla\left[\frac{\beta_i}{1+\beta_i^2}\right]\underline{\varepsilon} + \left[\frac{\beta_i}{1+\beta_i^2}\right](\nabla\cdot\underline{\varepsilon}) + \nabla\left[\frac{1}{1+\beta_i^2}\right]\cdot(\underline{\varepsilon}\times\hat{b})$$

$$+\left[\frac{1}{1+\beta_i^2}\right]\left[\hat{b}\cdot(\nabla\times\underline{\varepsilon}) - \underline{\varepsilon}\cdot(\nabla\times\hat{b})\right] + \nabla\left[\frac{1}{\beta_i(1+\beta_i^2)}\right]\cdot(\underline{\varepsilon}\cdot\hat{b})\hat{b}$$

$$+\left[\frac{1}{\beta_i(1+\beta_i^2)}\right]\left[(\nabla(\underline{\varepsilon}\cdot\hat{b}))\cdot\hat{b} + (\underline{\varepsilon}\cdot\hat{b})(\nabla\cdot\hat{b})\right] \qquad (3.2)$$

Expanding the last term in Equation (3.2):

$$\left[\frac{1}{\beta_i(1+\beta_i^2)}\right](\nabla(\underline{\varepsilon}\cdot\hat{b}))\cdot b$$

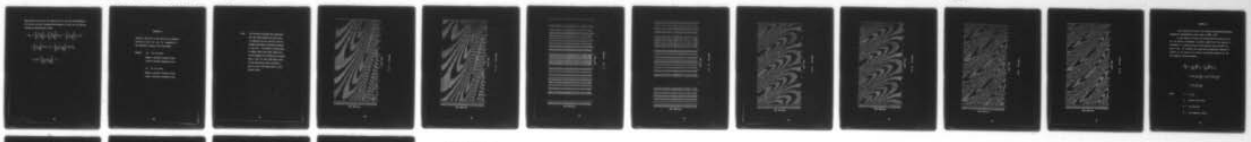
$$=\left[\frac{1}{\beta_i(1+\beta_i^2)}\right]\left[((\hat{b}\cdot\nabla)\underline{\varepsilon})\cdot\hat{b} + ((\underline{\varepsilon}\cdot\nabla)\hat{b})\hat{b}\right]$$

$$+ (\hat{b}\times(\nabla\times\underline{\varepsilon}))\cdot\hat{b} + (\underline{\varepsilon}\cdot(\nabla\times\hat{b}))\cdot\hat{b} \qquad (3.3)$$

AD-A066 839 WEATHER WING (1ST) HICKAM AFB HI F/G 4/2
THE ROLE OF ATMOSPHERIC TIDAL WINDS IN THE PRODUCTION OF IONOSP--ETC(U)
JUN 78 B D SPRINGER

UNCLASSIFIED 1WW-TN-78-1 NL

2 OF 2
AD
A066839





END
DATE
FILMED
5-79
DDC

Substituting (3.3) back into Equation (3.2), we have the expression for the ion velocity divergence/convergence arising from ion motions induced by electrostatic fields:

$$\nabla\cdot\underline{V}_i = \nabla\left[\frac{\beta_i}{1+\beta_i^2}\right]\cdot\underline{\varepsilon} + \left[\frac{\beta_i}{1+\beta_i^2}\right](\nabla\cdot\underline{\varepsilon}) + \nabla\left[\frac{1}{1+\beta_i^2}\right]\cdot(\underline{\varepsilon}\times\hat{b})$$

$$+ \left[\frac{1}{1+\beta_i^2}\right]\hat{b}\cdot(\nabla\times\underline{\varepsilon}) + \left[\frac{1}{\beta_i(1+\beta_i^2)}\right]\hat{b}\cdot((\hat{b}\cdot\nabla)\underline{\varepsilon}$$

$$+ (\underline{\varepsilon}\cdot\hat{b})\,\nabla\left[\frac{1}{\beta_i(1+\beta_i^2)}\right]\cdot\hat{b}$$

## APPENDIX 4

Graphical depiction of the vertical and temporal structure of the N-S and E-W components of the important E-region tidal wind modes.

Legends: (a) For E-W winds:

Numbers represent eastward winds.

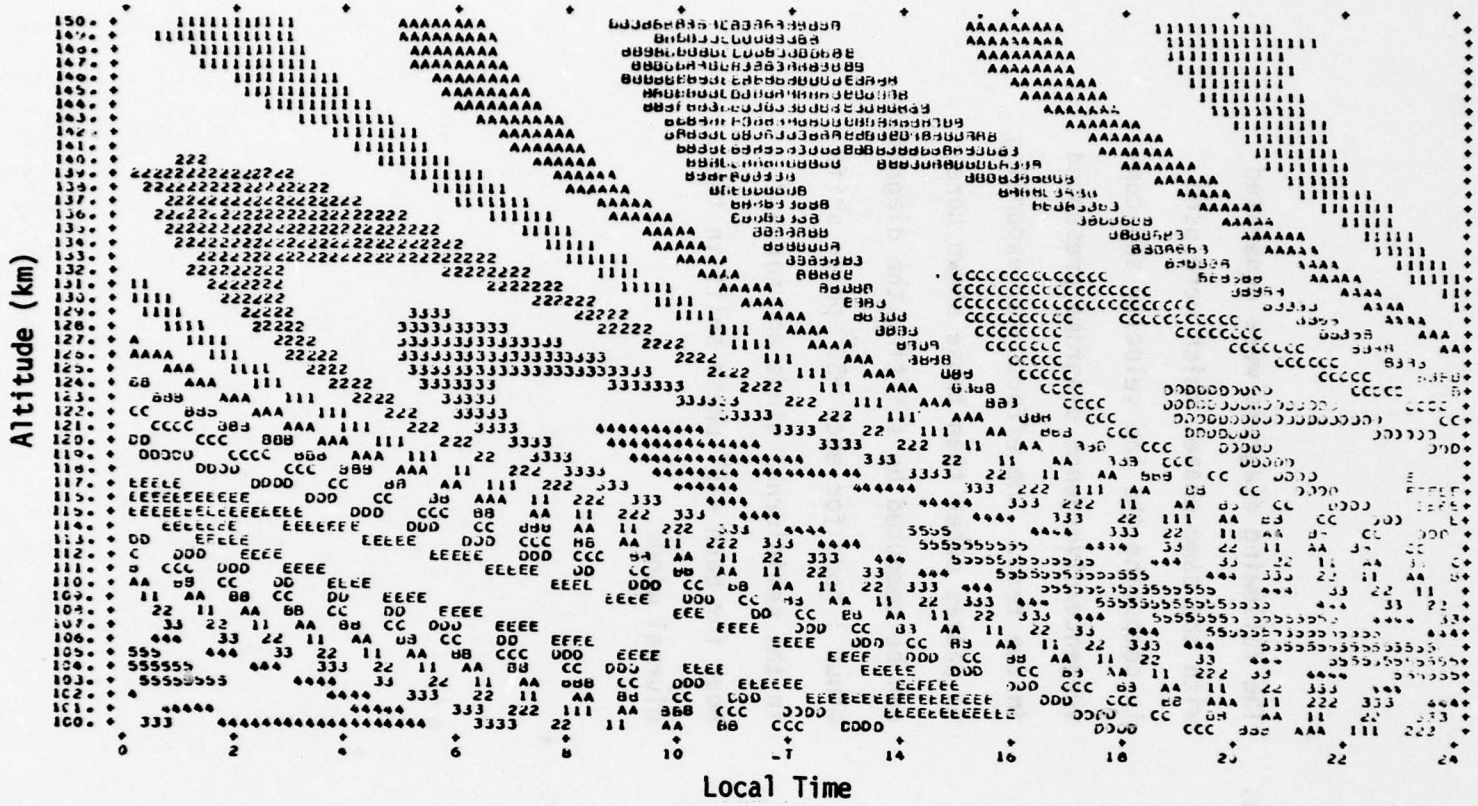
Letters represent westward winds.

(b) For N-S winds:

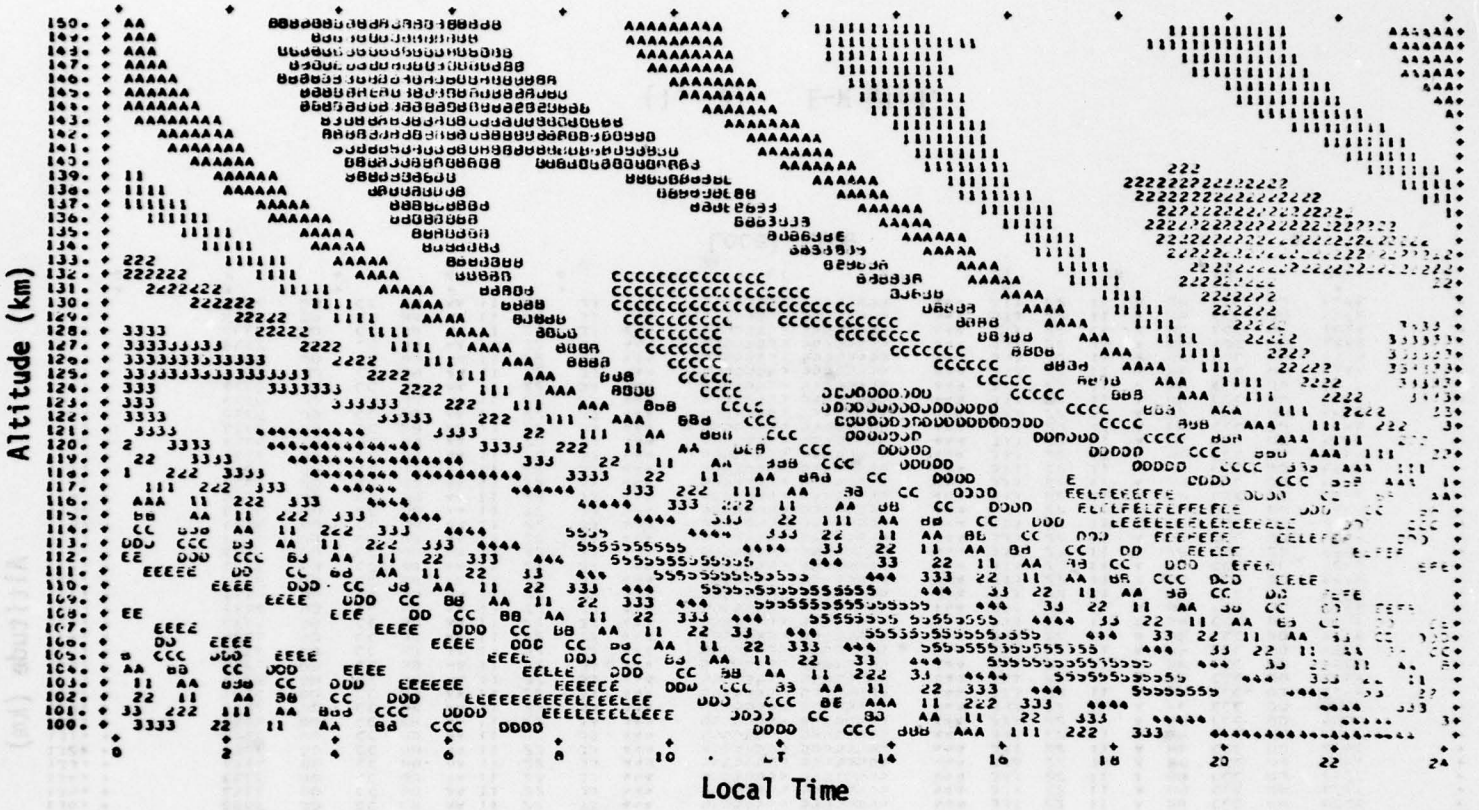
Numbers represent northward winds.

Letters represent southward winds.

Note: The following diagrams were generated with the same phases which were used in computing the ion velocity and convergence/divergence diagrams presented in the text. The effects corresponding to phases other than those shown here can be computed by shifting the diagrams minus 1 hour for each $+30^{o}$ phase shift in the semidiurnal winds and minus 1 hour for each $+15^{o}$ phase shift in the diurnal winds.



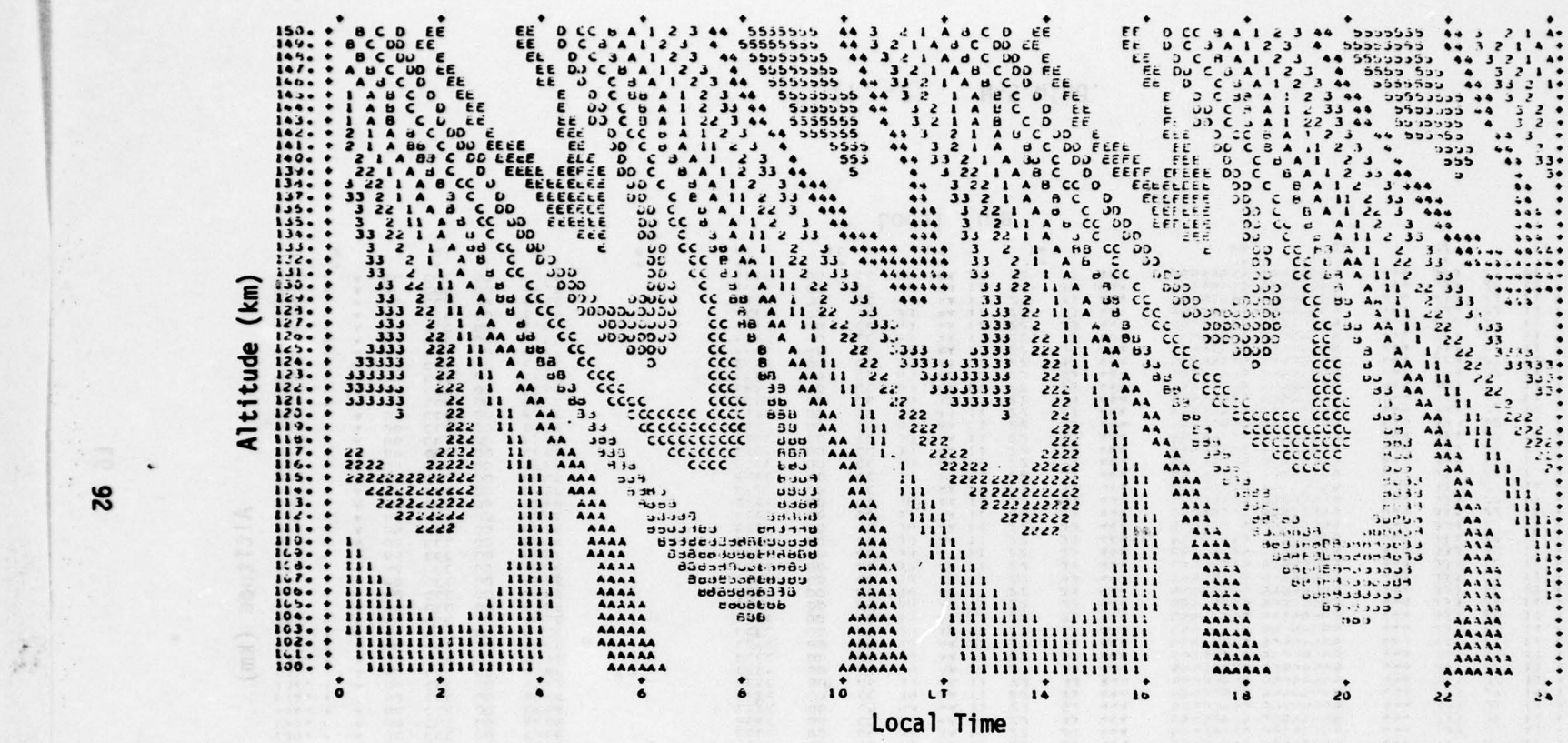

(1, 1) E-W wind.



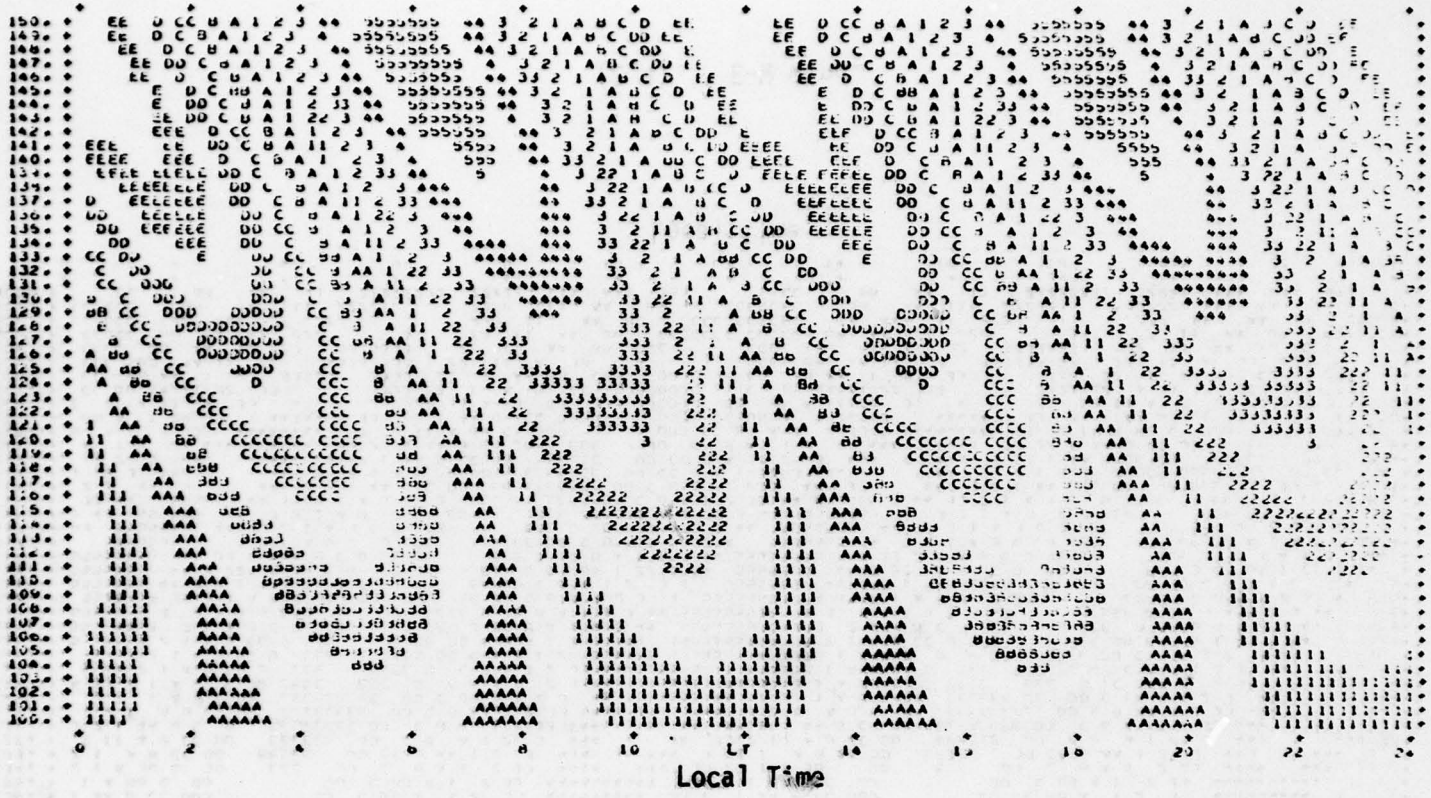

(1, 1) N-S wind.

(1, -2) E-W wind.

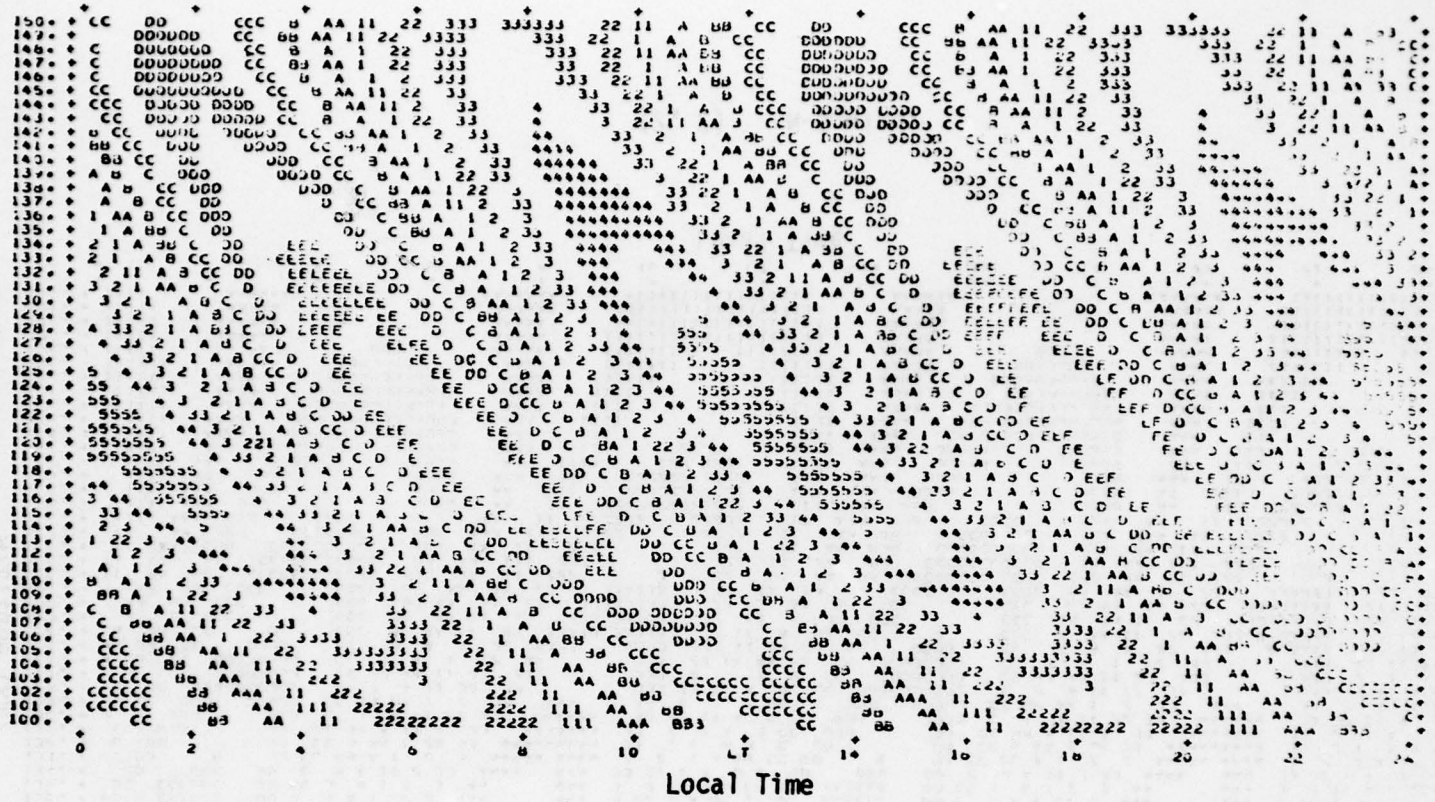
(1, -2) N-S wind.



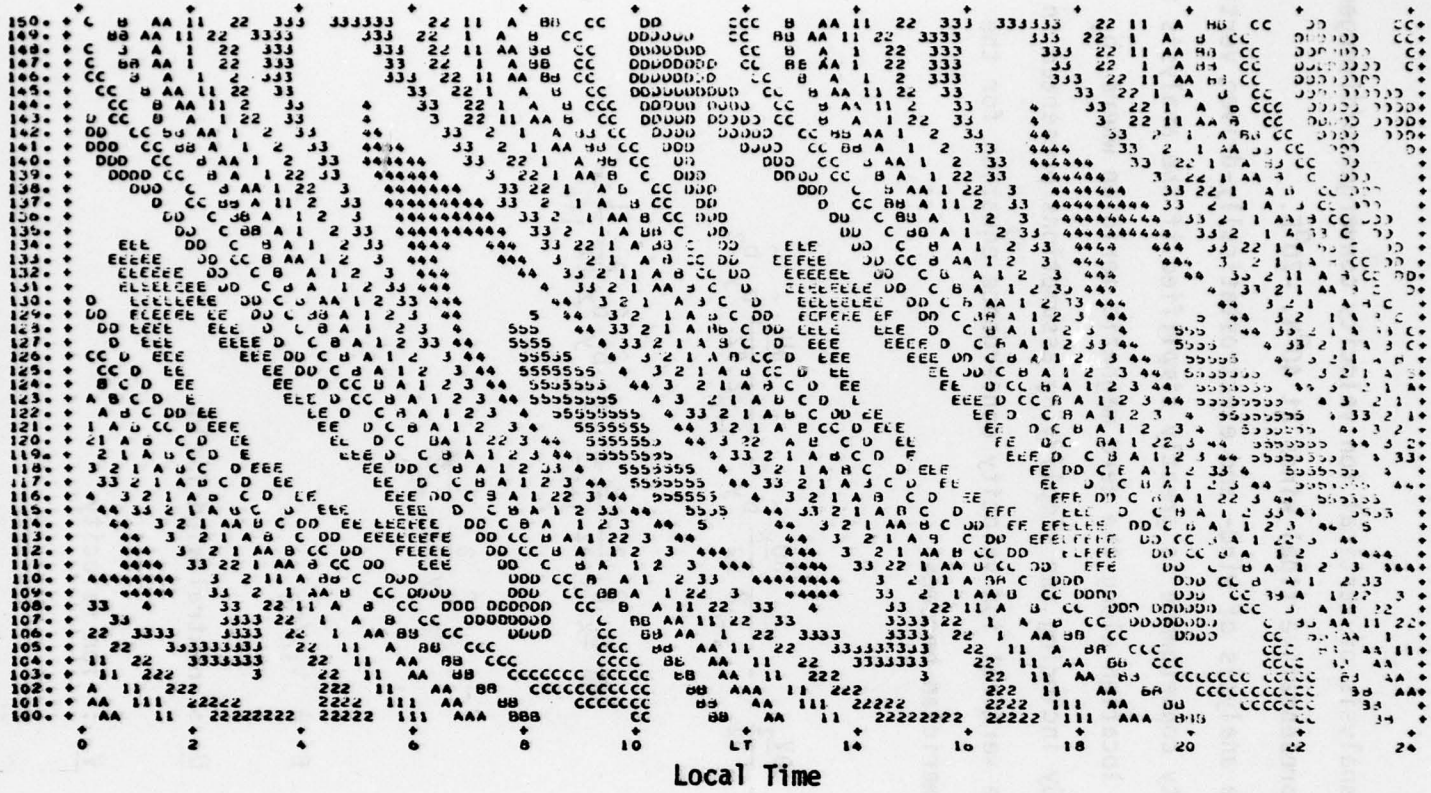

(2, 2) E-W wind.




(2, 2) N-S wind.




(2,4) E-W wind.




(2, 4) N-S wind.

## APPENDIX 5

Scale analysis of vertical ion velocity convergence/divergence produced by representative tidal winds at $40^{o}$N, $-70^{o}$E.

A scale analysis of wind- and electrostatically-driven vertical ion velocity convergence is greatly simplified if the analysis is performed at a location along the zero magnetic meridian where $\hat{b}_x$ equals zero. By including the simplifying assumptions presented in Chapter II, the vertical ion velocity convergence equation for the zero magnetic meridian becomes:

$$-\frac{\partial \underline{V}_z}{\partial z} = -\frac{\beta}{1+\beta^2}\frac{\partial \underline{U}_x}{\beta z}\hat{b}_y - \frac{1}{1+\beta^2}\frac{\partial \underline{U}_x}{\beta z}\hat{b}_y\hat{b}_z$$

$$+ \underline{U}_x \hat{b}_y \frac{\partial}{\partial z}\frac{\beta}{1+\beta^2} - \underline{U}_y \hat{b}_y \hat{b}_z \frac{\partial}{\partial z}\frac{1}{1+\beta^2}$$

$$- \underline{\xi}_x \hat{b}_y \frac{\partial}{\partial z}\frac{1}{1+\beta^2}$$

where $\beta \equiv \nu_{in}/\omega_i$

$\underline{U}$ : neutral wind field

$\underline{V}$ : ion velocity

$\hat{b}$ : unit magnetic vector

For $40^{o}$N, $-70^{o}$E, the magnetic field components are approximately

$$\hat{b}_x \approx 0., \quad \hat{b}_y \approx .36, \quad \hat{b}_z \approx -.93, \quad |\underline{B}| \approx .56 \text{ Gauss.}$$

For the purpose of scale analysis, a constant, horizontal, height-independent, E-W electric field of 1 mv/m has been specified. This equates to

$$\xi_x = \frac{E_x c}{|\underline{B}|} = 17.8 \text{ m/s} \quad .$$

The scale analysis has been performed for the five important ion convergence mechanisms for the altitudes of 120 and 150 km using $|\underline{U}_{max}| \approx 50$ m/s. The results follow.

(a) Scale analysis for 120 km (altitude) tidal winds:

$$\frac{\beta}{1+\beta^2} \approx .3 \quad \frac{1}{1+\beta^2} \simeq .08 \quad \left|\frac{\partial}{\partial z}\frac{\beta}{1+\beta^2}\right| \sim 3 \times 10^{-5}\ m^{-1} \quad \left|\frac{\partial}{\partial z}\frac{1}{1+\beta^2}\right| \simeq 3 \times 10^{-5}\ m^{-1}$$

$$-\frac{\partial \underline{V}_z}{\partial z} = -\frac{\beta}{1+\beta^2}\hat{b}_y\frac{\partial \underline{U}_x}{\partial z} - \frac{1}{1+\beta^2}\hat{b}_y\hat{b}_z\frac{\partial \underline{U}_y}{\partial z} + \underline{U}_x\hat{b}_y\frac{\partial}{\partial z}\frac{\beta}{1+\beta^2} - \underline{U}_y\hat{b}_y\hat{b}_z\frac{1}{1+\beta^2} - \underline{\xi}_x\hat{b}_y\frac{\partial}{\partial z}\frac{1}{1+\beta^2}$$



| Tidal wind mode | Term by term convergence ($sec^{-1}$) | | | | |
|---|---|---|---|---|---|
| (2, 2) | $7.6 \times 10^{-4}$ | $2.0 \times 10^{-4}$ | $2.5 \times 10^{-4}$ | $2.4 \times 10^{-4}$ | $1.9 \times 10^{-4}$ |
| (2, 4) | $1.8 \times 10^{-3}$ | $4.2 \times 10^{-4}$ | $5.4 \times 10^{-4}$ | $5.0 \times 10^{-4}$ | $1.9 \times 10^{-4}$ |
| (1, 1) | $1.1 \times 10^{-3}$ | $2.5 \times 10^{-4}$ | $4.4 \times 10^{-4}$ | $3.8 \times 10^{-4}$ | $1.9 \times 10^{-4}$ |
| (1, -2) | 0. | 0. | $5.4 \times 10^{-4}$ | $5.0 \times 10^{-4}$ | $1.9 \times 10^{-4}$ |

(b) Scale analysis for 150 km (altitude) tidal winds:

$$\frac{\beta}{1+\beta^2} \approx .3 \quad \frac{1}{1+\beta^2} \approx 1. \quad \left|\frac{\partial}{\partial z}\frac{\beta}{1+\beta^2}\right| \sim 10^{-5}\ m^{-1} \quad \left|\frac{\partial}{\partial z}\frac{1}{1+\beta^2}\right| \simeq 3 \times 10^{-6}\ m^{-1}$$

$$-\frac{\partial \underline{V}_z}{\partial z} = -\frac{\beta}{1+\beta^2}\hat{b}_y\frac{\partial \underline{U}_x}{\partial z} - \frac{1}{1+\beta^2}\hat{b}_y\hat{b}_z\frac{\partial \underline{U}_y}{\partial z} + \underline{U}_x\hat{b}_y\frac{\partial}{\partial z}\frac{\beta}{1+\beta^2} - \underline{U}_y\hat{b}_y\hat{b}_z\frac{\partial}{\partial z}\frac{1}{1+\beta^2} - \underline{\xi}_x\hat{b}_y\frac{\partial}{\partial z}\frac{1}{1+\beta^2}$$

| Tidal wind mode | Term by term convergence ($sec^{-1}$) | | | | |
|---|---|---|---|---|---|
| (2, 2) | $3.2 \times 10^{-4}$ | $1.0 \times 10^{-3}$ | $1.6 \times 10^{-4}$ | $4.9 \times 10^{-5}$ | $1.9 \times 10^{-5}$ |
| (2, 4) | $7.8 \times 10^{-4}$ | $2.2 \times 10^{-3}$ | $1.1 \times 10^{-5}$ | $3.2 \times 10^{-5}$ | $1.9 \times 10^{-5}$ |
| (1, 1) | $1.3 \times 10^{-4}$ | $3.2 \times 10^{-4}$ | $4.7 \times 10^{-5}$ | $1.2 \times 10^{-5}$ | $1.9 \times 10^{-5}$ |
| (1, -2) | 0. | 0. | $1.8 \times 10^{-4}$ | $5.0 \times 10^{-5}$ | $1.9 \times 10^{-5}$ |

## BIBLIOGRAPHY


Appleton, E.V. and R. Naismith (1947), The radio detection of meteor trails and allied phenomena, Physical Soc. of London Proc., 59, 461.

Behnke, R.A. and J.F. Vickrey (1975), Radar evidence for $Fe^+$ in a sporadic-E layer, Radio Sci., 10, 325.

Bossy, L.G. (1972), Comments on the first intensive period of observation of $E_S$ in Europe, Radio Sci., 7, 347.

Chapman, S. (1931a), The absorption and dissociative or ionizing effect of monochromatic radiation in an atmosphere on a rotating earth, Physical Soc. of London Proc., 43, 26.

Chapman, S. (1931b), The absorption and dissociative or ionizing effect of monochromatic radiation in an atmosphere on a rotating earth, Part II. Grazing incidence, Physical Soc. of London Proc., 43, 483.

Chapman, S. (1956), The electrical conductivity of the ionosphere: A review, Nuovo Cimento 4, 10, Sup. 4, 1385.

Dungey, J.W. (1956), The influence of the geomagnetic field on turbulence in the ionosphere, J. Atmos. Terr. Phys., 8, 39.

Dungey, J.W. (1959), Effect of a magnetic field on turbulence in an ionized gas, J. Geophys. Res., 64, 2188.

Gerson, N.E. (1955), Sporadic-E propagation, J. Atmos. Terr. Phys., 6, 113.

Goldberg, R.A. and A.C. Aikin (1973), Comet Encke: Meteor metallic ion identification by mass spectrometer, Science, 180, 294.

Istomin, V.G. (1963), Ions of extra-terrestrial origin in the ionosphere, Space Res., 3, 209.

Jacchia, L.G. (1971), Revised static models of the thermosphere and exosphere with empirical temperature profiles, Smithsonian Astrophysical Observatory Special Report Nr. 332, May, 1971.

Keneshea, T.J. and M.A. MacLeod (1970), Wind-induced modification of E-region ionization profiles, J. Atmos. Sci., 27, 981.

Lindzen, R.S. and S. Chapman (1969), Atmospheric tides, Space Sci. Rev., 10, 3.

MacDougall, J.W. (1974a), 110 km neutral wind patterns, Planet. Space Sci., 22, 545.

MacDougall, J.W. (1974b), Synthesis of sporadic-E patterns, in International Conference on Recent Advances in the Physics and Chemistry of the E-Region, 13-15 August 1974, Boulder, Colorado, p. 268.

MacLeod, M.A. (1964), Wind shear theory of sporadic-E. Project Firefly 1962-1963, AFCRL Environmental Res. Paper Nr. 15, p. 309.

MacLeod, M.A. (1966), Sporadic-E theory I. Collision-geomagnetic equilibrium, J. Atmos. Sci., 23, 96.

MacLeod, M.A. (1968), The influence of the neutral wind field on the distribution of ionization in the E-region, Met. Monographs, 9:31, p. 139, AMS, Boston.

MacLeod, M.A. (1969), E-region vertical neutral winds, Space Res., 9, 363.

MacLeod, M.A., T.J. Keneshea, and R.S. Narcisi (1972), A comparison of theoretical and experimental ion profiles for Project Aladdin (Abstract), EOS Transactions, AGU, 53, 464.

MacLeod, M.A., T.J. Keneshea, and B.W. Reinisch (1973), The Aladdin 2 ionosphere: A comparison of theoretical calculations with DIGISONDE observations (Abstract), EOS Transactions, AGU, 54, 381.

MacLeod, M.A., T.J. Keneshea, and R.S. Narcisi (1975), Numerical modelling of a metallic ion sporadic-E layer, Radio Sci., 10, 371.

Öpik, E.J. (1958), Physics of Meteor Flight in the Atmosphere, Interscience Publications, New York.

Philbrick, C.R., D. Golomb, S.P. Zimmerman, T.J. Keneshea, M.A. MacLeod, R.E. Good, B.S. Dandekar, and B.W. Reinisch (1974), The Aladdin 2 experiment, 2, Composition, Space Res., 14, 89.

Piddington, J.H. (1954), The motion of ionized gas in combined magnetic, electric and mechanical fields of force, Royal Astronom. Soc. Geophys. Supp., 114, 44.

Richmond, A.D. (1971), Tidal winds at ionospheric heights, Radio Sci., 6, 175.

Siebert, M. (1961), Atmospheric Tides, in Advances in Geophysics, Vol. 7, edited by H.E. Landsberg and J. VanMiegham, Academic Press, New York.

Smith, E.K. and J.W. Finney (1960), Pecularities of the ionosphere in the Far East: A report on I.G.Y. observations of sporadic E- and F-region scatter, J. Geophys. Res., 65, 885.

Smith, E.K. and S. Matsushita (1962), Ionospheric Sporadic E, MacMillan Co., New York.

Smith, L.G. (1970), A sequence of rocket observations of night-time sporadic-E, J. Atmos. Terr. Phys., 32, 1247.

Swider, W. (1969), Processes for meteoric elements in the E-region, Planet. Space Sci., 17, 1233.

Whitehead, J.D. (1961), The formation of the sporadic-E layer in the temperate zones, J. Atmos. Terr. Phys., 20, 49.

Whitehead, J.D. (1970), Production and prediction of sporadic-E, Rev. Geophys. Space Phys., 8, 65.

Wilkes, M.V. (1949), Oscillations of the Earth's Atmosphere, University Press, Cambridge, Mass.

Young, J.M., C.Y. Johnson, and J.C. Holmes (1967), Positive ion composition of a temperate latitude sporadic-E layer as observed during a rocket flight, J. Geophys. Res., 72, 1473.